

# Rheophysics of dense granular materials : Discrete simulation of plane shear flows

Frédéric da Cruz, Sacha Emam, Michaël Prochnow, Jean-Noël Roux and François Chevoir\*

*LMSGC, Institut Navier, 2 allée Kepler, 77 420 Champs sur Marne, France*

(Dated: February 2, 2008)

We study the steady plane shear flow of a dense assembly of frictional, inelastic disks using discrete simulation and prescribing the pressure and the shear rate. We show that, in the limit of rigid grains, the shear state is determined by a single dimensionless number, called inertial number  $I$ , which describes the ratio of inertial to pressure forces. Small values of  $I$  correspond to the quasi-static regime of soil mechanics, while large values of  $I$  correspond to the collisional regime of the kinetic theory. Those shear states are homogeneous, and become intermittent in the quasi-static regime. When  $I$  increases in the intermediate regime, we measure an approximately linear decrease of the solid fraction from the maximum packing value, and an approximately linear increase of the effective friction coefficient from the static internal friction value. From those dilatancy and friction laws, we deduce the constitutive law for dense granular flows, with a plastic Coulomb term and a viscous Bagnold term. We also show that the relative velocity fluctuations follow a scaling law as a function of  $I$ . The mechanical characteristics of the grains (restitution, friction and elasticity) have a very small influence in this intermediate regime. Then, we explain how the friction law is related to the angular distribution of contact forces, and why the local frictional forces have a small contribution to the macroscopic friction. At the end, as an example of heterogeneous stress distribution, we describe the shear localization when gravity is added.

PACS numbers: 45.70.Mg, 81.05.Rm, 83.10-y, 83.80.Fg

## I. INTRODUCTION

Due to their importance in geophysics (propagation of avalanches, migration of dunes, fault sliding) and in various industrial processes (handling of powders, granulates in civil and chemical engineering, food, pharmacy, tribology...), flows of granular materials are the focus of a large number of research, at the frontier between physics and mechanics [1, 2, 3, 4]. In order to predict propagation, flow-rate, jamming..., one of the main objectives of these “rheophysical” studies is to determine the rheological laws of those materials, based on their physical origin at the scale of the grains and of their interactions. One thus tries to express the stress tensor (and especially the pressure  $P$  and the shear stress  $S$ , positively counted) as a function of the shear rate  $\dot{\gamma}$  and other variables such as solid fraction  $\nu$ .

Granular materials are extremely various depending on the geometry of the grains (shape and size) and the nature of their interactions. We shall restrict our attention in the following to assemblies of cohesionless grains, slightly polydisperse, without interstitial fluid. This corresponds to macroscopic grains (diameter larger than hundred microns) in a fluid of low viscosity like air. The rheology is then only dictated by transfer of momentum and dissipation of energy taking place in direct contacts between grains and with the walls.

Depending on the conditions, these materials reveal various mechanical behavior, similar to elastoplastic

solids in the quasi-static regime, to dense gazes in the case of strong agitation, or to viscoplastic fluids when a flow is provoked. This paper is devoted to this intermediate regime, which is still not well understood. We shall first briefly recall the essential results for the two extreme regimes, quasi-static and collisional.

### A. Quasi-static regime

Dense, confined granular assemblies in extremely slow shear flow ( $\dot{\gamma} = 10^{-4}\text{s}^{-1}$  for sand) are usually described as solids abiding by elastoplastic constitutive laws [5, 6, 7, 8], or more general, incremental ones [9, 10]. A typical experiment consists in imposing a very slowly growing deviator (shear) strain to a sample prepared in mechanical equilibrium under an isotropic pressure. The material response is then independent of physical time, and involves volumetric strain, *i.e.*, dilatancy : loose samples contract, whereas dense ones expand. In dense samples, the shear deviator stress reaches a maximum (around shear strains of order 5%) and then decreases to a plateau. In a loose system, it increases monotonically to the same plateau value under the same confining stress. Meanwhile, the solid fraction approaches a limit which does not depend on its initial value either. It is therefore generally accepted that after a large enough shear strain (of order 10%), the material has reached a certain attractor state, called the *critical state* [11, 12], which does not depend on its initial arrangement. If larger shear strains are imposed, the critical state, with its internal structure adapted to shear flow in the limit of small velocities, will remain unaltered. The critical state is characterized by

---

\*Electronic address: Corresponding author : chevoir@lcp.fr

an internal friction angle  $\phi$ , defined as  $\tan \phi = S/P$  in a simple shear test, and by a critical solid fraction  $\nu_c$ . In the case of dense samples, the observation of the critical state is often precluded by the onset of shear localization, whereby the corresponding microstructure is limited to the material that is continuously sheared within thin bands.

Discrete numerical simulations have provided some additional information on the internal structure of granular materials as they approach their critical state. Thus the critical state is associated with specific values for coordination numbers and distribution of contact orientations ("fabric") [13]. Simulations also contributed to unravel the influence of contact elasticity on the macroscopic behavior. In the approach to the critical state, strains are essentially due to rearrangements, as contact networks break and repair. Macroscopic strains, with typical pressure levels and contact stiffnesses, as soon as they reach the  $10^{-4}$  range, originate in geometry changes and not in contact deformability [14, 15]. As a sample approaches its critical state, the gradually increasing anisotropy of the contact network allows it to support increasing deviator stresses [13]. Contact elasticity is essentially irrelevant in that regime, which can be modelled with rigid grains [16]. The internal friction angle  $\phi$  and the critical state solid fraction  $\nu_c$  are found to depend only negligibly on the confining pressure  $P$ . The slight dependence reported in experiments on sands [12] is likely due to features of the contact law, such as plasticity or breakage, which are usually not introduced in numerical simulations. In other words, the continuously sheared material can be modelled with the Coulomb criterion,  $S = P \tan \phi$ . If the *direction* of the imposed strain rate changes (*e.g.*, upon reversing the flow), then the system will leave its critical state and gradually approach another one, with different contact orientations [13].

Quasi-statically deformed granular systems are one limit case for the steady plane shear flows investigated in the present paper. Therefore, the results will be presented in the sequel in terms of an effective friction coefficient  $\mu^* = S/P$ , which should come close to  $\tan \phi$  in the limit of slow motion. Likewise, as appropriate for quasi-static granular rheology, we chose to control the lateral pressure rather than keeping the solid fraction fixed. Such options are further commented in the following.

## B. Collisional regime

In the dilute limit and/or for strong agitation, the grains interact through binary, instantaneous, uncorrelated collisions. Then, the generalization of the kinetic theory of dense gases to slightly inelastic grains [17, 18, 19, 20, 21] allows a hydrodynamical description. The stress components depend on the solid fraction and on the velocity fluctuations  $\delta v$  (which square defines the so-called *granular temperature*). In the two-dimensional geometry which we shall study in the following, the stress

components are homogeneous to a force divided by a length. For an assembly of disks of diameter  $d$  and mass  $m$ :

$$\begin{cases} P = F_P(\nu)m(\delta v/d)^2, \\ S = F_S(\nu)m(\delta v/d)\dot{\gamma}. \end{cases} \quad (1)$$

Solving a flow problem requires an additional equation of energy in which a dissipation rate  $\Gamma$  associated to inelastic collisions must be added to the usual terms:

$$\Gamma = F_\Gamma(\nu)m(\delta v/d)^3. \quad (2)$$

The dimensionless functions  $F_i(\nu)$  are completely expressed as functions of the pair correlation function at contact  $g_0(\nu)$ . In the dense limit ( $0.2 \leq \nu \leq 0.67$ ),  $F_i(\nu) \simeq A_i F(\nu)$ , with  $F(\nu) = \nu^2 g_0(\nu)$ . In two dimension,  $g_0(\nu) = (16 - 7\nu)/16(1 - \nu)^2$  [22]. The pre-factors  $A_i$  are well-known functions of the restitution coefficient  $e$  [19].

In the case of an homogeneous system, where the shear rate and the velocity fluctuations are uniform, the equation of energy reduces to a balance between the work of the shear stress and the dissipation:  $S\dot{\gamma} = \Gamma$ . This leads to  $\delta v = \dot{\gamma}d\sqrt{A_S/A_\Gamma}$ . Consequently, the stress components are equal to:

$$\begin{cases} P = G_P(\nu)m\dot{\gamma}^2, \\ S = G_S(\nu)m\dot{\gamma}^2, \end{cases} \quad (3)$$

where  $G_{P,S}(\nu) = B_{P,S}F(\nu)$  with  $B_P = A_P A_S/A_\Gamma$  and  $B_S = \sqrt{A_S^3/A_\Gamma}$ . We notice that the effective friction coefficient is a constant ( $\mu^* = \sqrt{A_S A_\Gamma/A_P^2}$ ), and that the solid fraction is a function of the dimensionless quantity  $I = \dot{\gamma}\sqrt{m/P}$  ( $\nu = G_P^{-1}(1/I^2)$ ). This collisional description is relevant in the dilute limit when the inertial effects dominate.

## C. Dense regime

In the intermediate regime, the solid fraction is close to a maximum solid fraction, so that one speaks of *dense flows*. Then, the grains interact both through enduring contacts and through collisions. There exists a contact network more or less percolating through the material, which is very fluctuating in space and time [23]. These flows are beyond the quasi-static regime, since the inertia of the grains (and so the shear rate) certainly comes into play. On the other hand, the assumption of binary, instantaneous, uncorrelated collisions of the kinetic theory is clearly in trouble. Due to the very strong correlations of motion and force, the theoretical description of those dense flows is very difficult and is still a matter of debate (see [24] for a recent review).

Advances have come in the last decade from the combination of discrete numerical simulations and experiments on model materials in simple geometry, confined or free surface flows (annular shear cell, vertical chute, inclined plane, heap-flow), and in various mechanical configurations (gravity, velocity or force imposed at a wall). A detailed review of these works can be found in [25].

Depending on the mechanical configurations, the flows are steady, intermittent, or even jam. A localization of the shear, with a width of a few grains, is also frequently observed near the walls or near the free surface, with exponential velocity profiles around. However, the heterogeneity of the stress distribution as well as the presence of walls makes the analysis of the constitutive law difficult.

#### D. Organization of the article

This is the reason why we have chosen to study this dense flow regime in steady homogeneous shear state. We have studied the simplest geometry, plane shear without gravity, in which the stress distribution is homogeneous inside the shear layer. Furthermore, we have prescribed both the shear rate and the pressure. Using discrete numerical simulations (“numerical experiments”), we have access to microscopic information, at the level of the grains and of the contact network, hardly measurable experimentally, and we are able to vary the parameters describing the grains and the shear state.

Sec. II is devoted to the description of the simulated system. Then in Sec. III we build a dimensionless number  $I$ , which, in the limit of rigid grains, describes the shear state and characterizes the progressive transition between the quasi-static and the dynamical regimes, called intermediate regime. We then show in Sec. IV that we obtain homogeneous states in term of structure (solid fraction), kinematics (shear rate) and stress distribution. In Sec. V, we measure the evolution of two macroscopic quantities (solid fraction and effective friction coefficient) as a function of  $I$  in the intermediate regime, from which we deduce the constitutive law. We then study the sensitivity of this constitutive law on the mechanical properties of the grains (restitution, friction and elasticity). The next sections are devoted to more detailed information, first on the fluctuations of the grain motion (Sec. VI), and then on the contact network (Sec. VII). Then, using those microscopic information, we explain in Sec. VIII how the friction law is related to the angular distribution of contact forces, and why the local frictional forces have a small contribution to the macroscopic friction. In the last Sec. IX, we study how the previous results are affected when the stress distribution becomes heterogeneous, in presence of gravity. For a more detailed account of the results, we refer to [26].

## II. SIMULATED SYSTEM

### A. Plane shear

The simulated system is two dimensional (Fig. 1). The granular material is a dense assembly of  $n$  dissipative disks of average diameter  $d$  and average mass  $m$ . Except in Sec. IV D 2, a small polydispersity of  $\pm 20\%$  is considered to prevent crystallization [22]. The mechanical properties of those grains are described by a friction coefficient  $\mu$ , a restitution coefficient in binary collisions  $e$  and elastic stiffness coefficients  $k_n$  and  $k_t$ .

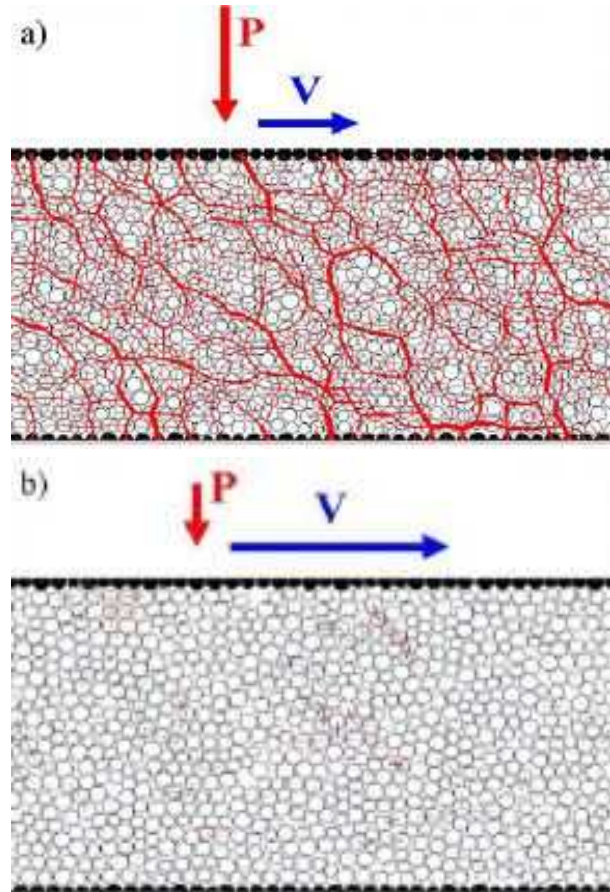


FIG. 1: (Color online) Plane shear : (a) Quasi-static regime ( $I = 10^{-2}$ ) (b) Dynamic regime ( $I = 0.2$ ). (Black grains constitute the rough walls. The line widths are proportional to the intensity of the normal force between grains).

The granular material is submitted to a plane shear, without gravity (except in Sec. IX), so that the stress distribution is uniform. The material is sheared between two parallel rough walls, distant of  $H$ . One of the wall is fixed, while the other moves at the prescribed velocity  $V$ . We call  $x$  the flow direction and  $y$  the transverse direction. Periodic boundary conditions are applied along the flow direction, and we call  $L$  the length of the simulation box (always larger than 40 grains). The wall roughness is

made of contiguous grains sharing the characteristics of the flowing grains (same polydispersity and mechanical properties - no rotation).  $y = 0$  corresponds to the center of the glued grains on the fixed wall.

An important feature of our simulation is that the normal stress  $\Sigma_{yy}$  is prescribed, as usual in practice. We shall see in the following (Sec. IV B 2) that the normal stress components  $\Sigma_{xx}$  and  $\Sigma_{yy}$  are equal, so that  $\Sigma_{yy}$  is equal to the pressure  $P = (\Sigma_{xx} + \Sigma_{yy})/2$ . The control of the pressure  $P$  is achieved by allowing the dilatancy of the shear cell along  $y$  ( $H$  is not fixed), through the vertical motion  $\dot{H}$  of the moving wall. The evolution of  $H$  is given by :  $\dot{H} = (P - P_w)L/g_p$ , where  $g_p$  is a viscous damping parameter, and  $P_w$  is the normal stress exerted by the grains on the moving wall. Steady state corresponds to  $\langle P_w \rangle = P$ .

The parameters of the simulated system are summarized in Tab. I (anticipating on Sec. III, we indicate the value of the dimensionless parameters  $g_p/\sqrt{mk_n}$  and  $I$ ).

$n$	$L/d$	$H/d$	$g_p/\sqrt{mk_n}$	$I$
900 - 5000	40 - 100	20 - 100	1	$6.10^{-4} - 0.3$

TABLE I: *List of system parameters.*

Due to its interest in rheology and more specifically in tribology (third body) and in geophysics (sliding of faults at the origin of earthquakes), this plane shear geometry has already been the subject of numerous discrete simulation studies [23, 27, 28, 29, 30, 31, 32, 33, 34, 35, 36, 37, 38, 39, 40, 41, 42], to which we shall refer in the following. Those studies are generally two-dimensional (except [32, 37, 39]), with a prescribed velocity (except [40] where the shear stress is prescribed), with a fixed volume (except [23, 29, 31, 38, 40] where the pressure is prescribed), and between rough walls (except [23, 28, 32, 39, 42] where periodic boundary conditions are applied along the transverse direction).

## B. Contact law

Let us consider two grains  $i$  and  $j$  in contact, of diameter  $d_{i,j}$ , mass  $m_{i,j}$ , centered at position  $\vec{r}_{i,j}$ , with velocity  $\vec{v}_{i,j}$  and rotation rate  $\omega_{i,j}$ . Let  $\vec{n}_{ij}$  denote the normal unit vector, pointing from  $i$  to  $j$  ( $\vec{n}_{ij} = \vec{r}_{ij}/\|\vec{r}_{ij}\|$ ) with the notation  $\vec{r}_{ij} = \vec{r}_j - \vec{r}_i$ , and  $\vec{t}_{ij}$  a unit tangential vector such that  $(\vec{n}_{ij}, \vec{t}_{ij})$  is positively oriented. We call  $\vec{F}_{ij} = N_{ij}\vec{n}_{ij} + T_{ij}\vec{t}_{ij}$  the contact force exerted on the grain  $j$  by the grain  $i$ . The *contact law* relates the contact force to the corresponding components of relative displacements and/or velocities. The relative velocity at the contact point is equal to  $\vec{V}_{ij} = \vec{v}_i - \vec{v}_j + 1/2(d_i\omega_i + d_j\omega_j)\vec{t}_{ij}$ . Its normal component

$V_{ij}^N = \vec{n}_{ij} \cdot \vec{V}_{ij}$  is the time derivative of the normal deflection of the contact (or apparent ‘‘interpenetration’’ of undeformed disks),  $h_{ij} = (d_i + d_j)/2 - \|\vec{r}_{ij}\|$ . Its tangential component  $V_{ij}^T = \vec{t}_{ij} \cdot \vec{V}_{ij}$  is the time derivative of the tangential relative displacement  $\delta_{ij}$ . (Let us note that the definition of  $\delta_{ij}$  as a scalar quantity automatically accounts for the material transport of strain in the contact region, as  $\vec{t}_{ij}$  moves with the pair in contact).

The normal contact force is the sum of two contributions, an elastic one  $N^e$  and a viscous one  $N^v$  :  $N_{ij} = N_{ij}^e + N_{ij}^v$ .

### 1. Viscoelasticity

Keeping in mind that contacts have to close to transmit forces ( $\vec{F}_{ij} = \vec{0}$  if  $h_{ij} < 0$ ) the linear (unilateral) elastic law reads

$$N_{ij}^e = k_n h_{ij}. \quad (4)$$

Eqn. (4) involves a constant normal stiffness coefficient  $k_n$ , the value of which is independent of disk radii.

The normal viscous force opposes the relative approaching or receding velocity :

$$N_{ij}^v = \zeta_{ij} \dot{h}_{ij}. \quad (5)$$

$\zeta_{ij}$  is related to the normal restitution coefficient  $e$  in a binary collision, and chosen such that  $e$  is constant for all contacting pairs, whence

$$\zeta_{ij} = \frac{-2 \ln e}{\sqrt{\pi^2 + \ln^2 e}} \sqrt{\frac{m_{ij}}{k_n}}. \quad (6)$$

where  $m_{ij} = m_i m_j / (m_i + m_j)$ .

Physically, Eqn. (4) can be regarded as a simplified version of the Hertz law [43],  $N^e \propto h^{3/2}$ , while the viscous dissipation might stem from the visco-elasticity of the grain material [44].

The total normal force might be either repulsive or attractive, due to the viscous contribution. We could check that setting  $N_{ij}$  to zero whenever it becomes attractive ( $N_{ij} < 0$ ) has but a negligible effect on the simulation results [45].

### 2. Friction

The Coulomb condition in the contacts involves the coefficient of friction between grains  $\mu$ , and is enforced with the sole elastic part of the normal force :

$$|T_{ij}| \leq \mu N_{ij}^e. \quad (7)$$

polydispersity	$\mu$	$e$	$k_t/k_n$	$\kappa$
$\pm 20\%$	0-0.8	0.1-0.9	0.5	$10^4$

TABLE II: *List of material parameters.*

To this end, the tangential component of the contact force is related to the *elastic part*  $\delta_{ij}^e$  of the relative tangential displacement  $\delta_{ij}$ ,

$$T_{ij} = k_t \delta_{ij}^e, \quad (8)$$

with a tangential stiffness coefficient  $k_t$ .  $\delta_{ij}^e$  is defined by :

$$\frac{d\delta_{ij}^e}{dt} = \begin{cases} 0 & \text{if } |T_{ij}| = \mu N_{ij}^e \text{ and } T_{ij} V_{ij}^T > 0 \\ V_{ij}^T & \text{otherwise} \end{cases} \quad (9)$$

The contact is termed “sliding” in the first case in Eqn. (9) (the condition that  $T_{ij}$  and  $V_{ij}^T$  share the same sign ensuring a positive dissipation due to friction) and “rolling” in the second case.  $k_t$  is of the same order of magnitude as  $k_n$  [43]. As it has a very small influence on the results [39], it was fixed to  $k_n/2$  in all our calculations.

Table II gives the list of material parameters (anticipating on Sec. III, we indicate the value of the dimensionless parameter  $\kappa$ ). Most simulations were done with  $e = 0.1$  and  $\mu = 0.4$ , which implies a rather strongly dissipative material, favors dense flows, and seems fairly realistic. Other friction coefficients and restitution coefficients were also studied.

### C. Simulation method

The interaction law being chosen, numerical simulations are carried out with the molecular dynamics method, as in refs. [46, 47, 48]. The equations of motion are discretized using a standard procedure (Gear’s order three predictor-corrector algorithm [49]). The time step is a small fraction (1/100) of the duration  $\tau_c$  of a binary collision between two grains of mass  $m$  ( $\tau_c = \sqrt{m(\pi^2 + \ln^2 e)/(4k_n)}$ ).

## III. DIMENSIONAL ANALYSIS

In order to analyze the results, we recall the list of parameters describing the material and the shear state. The grains are described by their size  $d$ , mass  $m$ , stiffness parameters  $k_n$  and  $k_t$ , and coefficients of restitution  $e$  and of friction  $\mu$ . The shear state is described by the prescribed pressure  $P$  and the average shear rate  $V/H$ , and by the viscous damping parameter  $g_p$ . In the following, we shall express the results in the natural units

of the simulated system. If the length and mass scales  $d$  and  $m$  are obvious, there are three candidates for the time scale : the shear time  $1/\dot{\gamma}$ , the inertial time  $\sqrt{m/P}$  (that is to say the characteristic displacement time of a grain of mass  $m$  submitted to a pressure  $P$ ), and the collision time  $\tau_c$ . However, dimensional analysis predicts that the behavior will only depend on six dimensionless numbers. Apart from  $\mu$ ,  $e$  and  $k_t/k_n$ , we propose the following choice of the three other dimensionless numbers:

- i) The first  $g_p/\sqrt{mk_n}$  is associated to the normal motion of the wall controlling the pressure. A small value signifies that the time scale of the fluctuations of  $H$  is imposed by the material rather than the wall, and that the wall “glues” to the material.
- ii) The second  $\kappa = k_n/P$  is associated to the rigidity of the grains. It is inversely proportional to the normal deflection  $h$  of the contacts for a confining pressure  $P$ .
- iii) The third  $(V/H)\sqrt{m/P}$  describes the shear state, through a combination of the three global parameters (velocity  $V$ , pressure  $P$  and height  $H$ ), which means that it is not necessary to vary independently those three parameters.

The first dimensionless number is equal to 1 in our simulations. We have not studied its influence, but consider that it is small in this range. We shall not refer to it in the following.

Most of our calculations are restricted here to the limit of rigid grains [42],  $\kappa \rightarrow \infty$ , as we chose  $\kappa = 10^4$  (unless specified otherwise, as in Sec. IV D 2). From studies in the quasi-static regime, this value is known to be large enough for the coordination number to show little variation as  $\kappa$  is further increased (see, however, Sec. VII A). With  $\kappa = 10^4$ , the typical ratio  $h/d \propto \kappa^{-1}$  is so small that elastic deflections  $h$  stay negligible in comparison with the gaps between neighboring grain surfaces that determine the amplitude of rearrangement events [14] (a more stringent condition than  $h \ll d$ ). In practice, a suitable definition of  $\kappa$  for particles with Hertzian contacts (such that  $h/d \propto \kappa^{-1}$  with a coefficient of order 1) is  $\kappa = (E/P)^{2/3}$ , where  $E$  is the Young modulus of the material the grains are made of. For glass ( $E = 70$  GPa) and  $P = 10$  kPa (the pressure due to the weight of a 50 cm thick layer) one has  $\kappa \simeq 37000$ .

### A. Inertial number $I$

In the following, we study in detail the influence of the third dimensionless number. It is a global number  $I_g$ , at the scale  $H$  of the sheared layer. Replacing the global shear rate  $V/H$  by the local one  $\dot{\gamma}$  defines the local analogous quantity :

$$I = \dot{\gamma} \sqrt{\frac{m}{P}}. \quad (10)$$

As the ratio of inertial to shear times,  $I$  measures the inertial effects, and will be called *inertial number* in the following. This number already appeared in the collisional regime (Sec. IB). In a three dimensional situation, the inertial number is equal to  $\dot{\gamma}\sqrt{m/Pd}$ . We notice that, introducing the mass density  $\rho_g$  of the grains, the definition  $I = \dot{\gamma}d\sqrt{\rho_g/P}$  does not depend on the dimensionality of the system.

In a homogeneous system, without sliding velocity at the wall, both definitions, global and local, are equivalent. But in a heterogeneous system, it is necessary to take into account the variations of the local inertial number along  $y$ :  $I(y) = \dot{\gamma}(y)\sqrt{m/P(y)}$ .

We are going to show that this dimensionless number might well be the fundamental quantity to describe the rheology of granular materials. First of all, it is the correct quantity to characterize the flow regime. Thus, the terminology of “slow” versus “rapid” granular flows is not correct, since it is necessary to combine shear rate and pressure to characterize the inertial effects. A small value of  $I$  (small  $\dot{\gamma}$  and/or large  $P$ ) corresponds to a regime where the grain inertia is not relevant : this is the “quasi-static” regime (Fig. 1 (a)). Inversely, a large value of  $I$  (small  $P$  and/or large  $\dot{\gamma}$ ) corresponds to the “inertial” or “dynamical” regime, which may be described by the kinetic theory (Fig. 1 (b)). Varying  $I$  allows to study the progressive transition between those two regimes. The range of inertial number which we have studied goes from  $6 \cdot 10^{-4}$  to 0.3.

## B. Comments

It might be pointed out that the inertial number is directly related to the *Bagnold number*  $Ba$ , which can be defined as the ratio of the typical kinetic energy  $m(d\dot{\gamma})^2$  of one grain to the characteristic frictional dissipation  $\mu Pd^2$  [2]. Some authors [28, 39] chose to control the solid fraction  $\nu$  rather than the pressure, and therefore, rather than  $I$  and  $\kappa$ , used the pair of dimensionless numbers  $\nu$  and  $\alpha = \dot{\gamma}/\sqrt{k_n/m} = I/\sqrt{\kappa}$ , as variables characterizing the state of the granular material in steady homogeneous shear flow. The latter dimensionless combination  $\alpha$  may be viewed as the ratio of the collision time to the shearing time, or as the shearing velocity divided by the sound velocity (Mach number [39]). Both choices are perfectly legitimate, as dimensional analysis predicts either  $S/P = f_1(I, \kappa)$  and  $\nu = f_2(I, \kappa)$ , or  $S/P = f_3(\nu, \alpha)$  and  $P/k_n = f_4(\nu, \alpha)$ , both results being equally valid. The choice of  $I$  and  $\kappa$  can however be deemed more convenient for several reasons. First, the variation of the results with  $\nu$ , regarded as a control parameter, is extremely fast. Each material possesses a critical packing fraction  $\nu_c$ , in the sense of Sec. IA, above which it does not flow, unless stresses are so large that the elastic compression of contacts compensates for the difference  $\nu - \nu_c$ . Below  $\nu_c$ , on the other hand, a continuously sheared granular system is free to flow with a negligible shear stress,

unless the velocity is high enough to build a significant pressure. One should therefore monitor  $\nu$  with great accuracy to observe ordinary stress levels. This renders the comparisons between different granular systems difficult, as one would need to know in advance the value of the critical density for each of them. Furthermore, the limit of rigid grains becomes singular, as all values of  $\nu$  above  $\nu_c$  are strictly forbidden for  $\dot{\gamma} \neq 0$ , while the properties of shear flows with  $\nu < \nu_c$  simply scale with  $\dot{\gamma}$  in that limit [42]. Conversely, if one uses  $I$  and  $\kappa$  as control parameters, no singularity enters any of the relevant results in the  $I \rightarrow 0$  or  $\kappa \rightarrow \infty$  limits, and different materials should exhibit similar (if not quantitatively identical) behaviors for the same values of these parameters (which thus define roughly “corresponding states”). It should also be pointed out that experimental conditions usually determine stress levels, rather than densities.

## IV. HOMOGENEOUS SHEAR STATE

### A. Preparation of steady shear states

The first kind of preparation (which has been used most of the time) consists in starting from an initial configuration where the disks are randomly deposited without contact and at rest between the two distant walls, which provides an average solid fraction of 0.5, and then in applying the pressure to the wall while slowly shearing the granular material. When the pressure on the walls reaches the prescribed value, the prescribed velocity is applied.

The second kind of preparation consists in starting from a very high solid fraction (of the order of 0.8), obtained by a random deposit followed by a cyclic compaction with frictionless grains, and then to introduce friction between grains and to start the shear with the prescribed velocity and pressure.

The two kinds of preparation allow to start either from a loose state (the first case), or from a dense state (the second case). Occasionally, we have used a third kind of preparation consisting in starting from localized shear states near one of the walls (obtained by applying gravity, see Sec. IX).

We then look for a steady flow, characterized by constant time-averaged quantities of the flowing layer, like kinetic energy and solid fraction. We have observed that, after a sufficient amount of time, the three kinds of preparation lead to the same shear state. We deduce that there is no influence of the preparation on the steady flow characteristics.

All the simulations converge to an average steady state. But the relative fluctuations of the measured quantities can be very different. In the following, we consider that the shear state is continuous if they are smaller than 10%. Otherwise, the flow is called intermittent. This happens in the quasi-static regime, for  $I \leq 0.001$  (see Sec. VIA).

When a steady state is reached, the simulation is carried on during a sufficient amount of time  $\Delta t$ , so that the typical relative displacement of two neighboring layers is larger than ten grains ( $\dot{\gamma}\Delta t \geq 10$ ). In this steady state, we consider that the statistical distribution of the quantities of interest (structure, velocities, forces. . .) are independent of  $t$  and  $x$ , so that we average both in space (along  $x$ ) and in time (considering 200 time steps distributed over the period  $\Delta t$ ).

## B. Profiles

We now show that the granular material is completely sheared and that the shear is homogeneous. To this end, we analyze the profiles of solid fraction, velocity and stress components. Typical profiles are shown in Fig. 2.

### 1. Solid fraction and velocity

The profiles of solid fraction  $\nu(y)$  and shear rate  $\dot{\gamma}(y)$  are strongly oscillating near the walls, but we may consider them as approximately constant in the central part of the sheared layer (Fig. 2 (a) and (b)). This allows to define average solid fraction  $\nu$  and shear rate  $\dot{\gamma}$ .

We notice that those profiles obtained for controlled pressure are in agreement with the one measured at fixed volume [50].

We have also measured the profile of average rotation rate  $\omega(y)$  (Fig. 2 (b)), and observed, as in other flows and quasi-static deformations [32, 51, 52, 53, 54, 55], the following relation  $\omega(y) = -\frac{1}{2}\dot{\gamma}(y)$ .

### 2. Stress tensor

The stress tensor  $\underline{\underline{\Sigma}}$  is the sum of two contributions [56]:

$$\underline{\underline{\Sigma}} = \underline{\underline{\Sigma}}^c + \underline{\underline{\Sigma}}^f. \quad (11)$$

The first term (“contact”), usual in static of granular materials, is associated to contact forces between grains [57, 58]. The second term (“fluctuations”), usual in fluid mechanics (Reynolds tensor), is associated to the velocity fluctuations of the grains  $\delta\vec{v}_i$ :

$$\begin{cases} \underline{\underline{\Sigma}}^c = \frac{1}{LH} \sum_{i<j} \vec{F}^{ij} \otimes \vec{r}^{ij} \\ \underline{\underline{\Sigma}}^f = \frac{1}{LH} \sum_{i=1}^n m_i \delta\vec{v}_i \otimes \delta\vec{v}_i \end{cases} \quad (12)$$

A third contribution, associated to the rotation of the grains, has been introduced in [59]. We have observed that it is usually insignificant [26], so that we shall not discuss it in the following. We discuss here the total contribution and shall analyze the two contributions in Sec. VI.

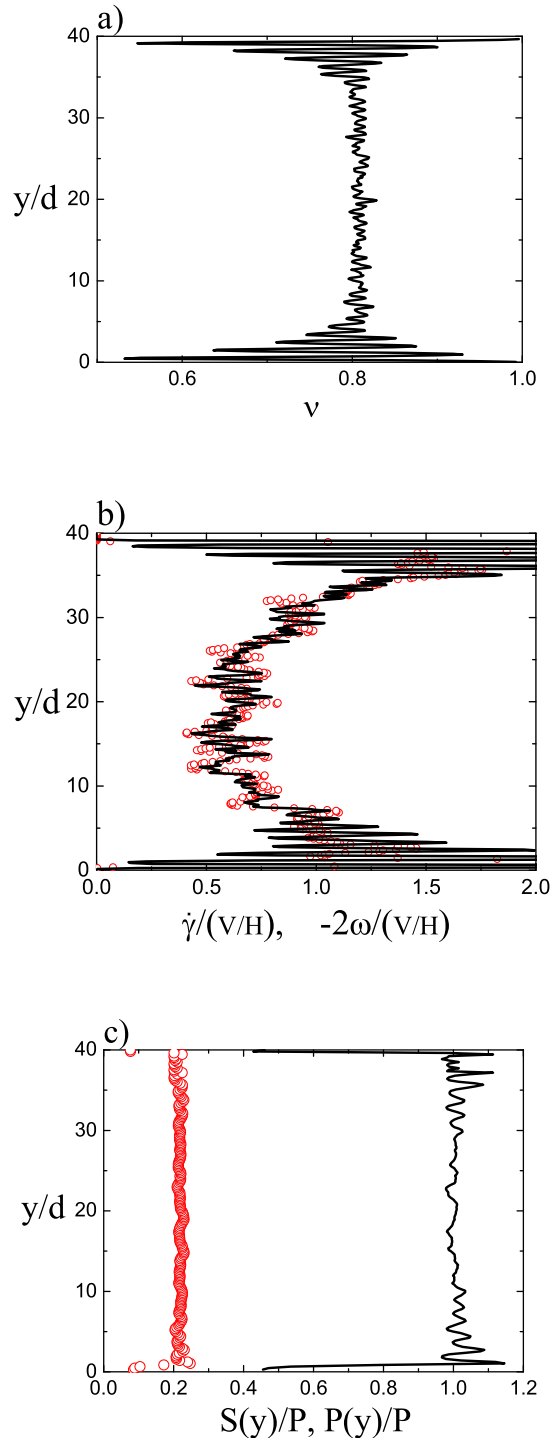


FIG. 2: (Color online) Homogeneous shear state : (a) Solid fraction  $\nu(y)$ , (b) Shear rate  $\dot{\gamma}(y)$  (—) and rotation velocity  $-2\omega(y)$  ( $\circ$ ), (c) Pressure  $P(y)$  (—) and shear stress  $S(y)$  ( $\circ$ ) ( $V = 1, P = 25, H/d \approx 40, e = 0.1, \mu = 0.4$ ).

Using the same averaging methods than for solid frac-

tion and velocities [55], it is possible to calculate the profiles of the different components of the stress tensor. We observe that  $\Sigma_{xx} \simeq \Sigma_{yy}$ , like for dense flows down inclined planes [42, 47, 55]. Consequently the pressure  $P = (\Sigma_{xx} + \Sigma_{yy})/2 \simeq \Sigma_{yy}$ . In the following we call  $S = -\Sigma_{xy}$ . The Fig. 2 (c) shows the profiles  $P(y)$  and  $S(y)$ . Those components are approximately constant along  $y$ , as expected.

### 3. Inertial number

From the profiles of shear rate and pressure inside the flow, we deduce the profile of inertial number  $I(y)$ . It is approximately constant in the center of the sheared layer, so that it is possible to define an average  $I$  (in Fig. 2  $I \approx 0.004$ ).

### C. Behavior near the walls

Particular behaviors of solid fraction, velocity and stress components are observed near the walls. First, the walls induce a structuration of the granular material in the 5 first layers, evidenced by the oscillations of the solid fraction and shear rate. Second, the frustration of the rotation of the flowing grains in contact with the rotationless glued grains of the roughness induces a sudden variation of the average rotation. This may be responsible for the difference of normal stress components ( $\Sigma_{xx} \neq \Sigma_{yy}$ ) in the first two layers (not shown). Third the granular material is agitated by the roughness, which increases the shear rate (see Sec. VI). Consequently, all the average quantities are measured in the central part of the sheared layer, excluding the 5 first layers near the walls and  $H$  is chosen large enough so as to limit those wall effects.

However, we have tested the homogeneity of the shear in the case of a thin layer ( $H/d \approx 5$ ) [26]. Then the granular material is structured on its whole width and completely sheared. We shall come back to this case in the following.

### D. Limits of homogeneity

Even when starting from a localized velocity profile, we have observed a relaxation toward a homogeneous shear state. This observation is in contrast with other studies, where a shear localization is observed [27, 35, 37, 38]. In our simulations, we have observed signs of localization in the quasi-static regime where the flow becomes intermittent (Sec. VI), and once the stress distribution becomes heterogeneous (Sec. IX). We now briefly discuss two other factors of localization, which are associated to the granular material itself, the monodispersity and the softness of the grains.

### 1. Influence of the polydispersity

In the case of a very small polydispersity ( $\leq 1\%$ ), we have observed [26] that the granular material crystallizes near the walls. The shear zone then reduces to a ten diameters thick central layer, where the velocity profile is linear. When the polydispersity is increased, the shear zone extends first to the moving wall (5%) then to the whole layer (10%).

### 2. Influence of the rigidity

We expect that the correlation length of the strain field becomes smaller when the grains become softer. This might be responsible for a localization of the shear near the moving wall. In order to test this idea, we have studied the influence of the dimensionless rigidity number  $\kappa$  in a large system ( $H/d = 100$ ) for  $I_g = 2 \cdot 10^{-4}$ . For  $\kappa = 1000$ , we observe homogeneous shear states, whereas for  $\kappa = 40$ , the shear becomes localized [26].

## V. CONSTITUTIVE LAW

Those homogeneous states are a great advantage to measure the constitutive law of dense granular flows. This would be much more difficult in other flow geometries (annular shear, vertical chute, inclined plane, heap-flow...) [25] where the flow is heterogeneous, so that the constitutive law cannot be identified on the whole flowing layer, but should be studied locally, in the presence of gradients.

In those homogeneous states where the inertial number  $I$  is prescribed, the solid fraction and the shear stress adjust in response to  $I$ . Consequently, we shall first measure the dependences of two fundamental dimensionless quantities, the solid fraction and the effective friction coefficient, as functions of  $I$ . Then we will study the influence of the mechanical properties of the grains, the coefficients of restitution  $e$  and friction  $\mu$ .

### A. Dilatancy law

We call ‘‘dilatancy law’’ the variations of the average solid fraction  $\nu$  as a function of the inertial number  $I$  (Fig. 3). We observe that  $\nu$  decreases approximately linearly with  $I$ , starting from a maximum value  $\nu_{max}$  :

$$\nu(I) \simeq \nu_{max} - aI, \quad (13)$$

with  $\nu_{max} \simeq 0.81$  and  $a \simeq 0.3$  (for  $\mu = 0.4$ ). The error bar (independent of  $I$ ) corresponds to the statistical dispersion inside the layer.



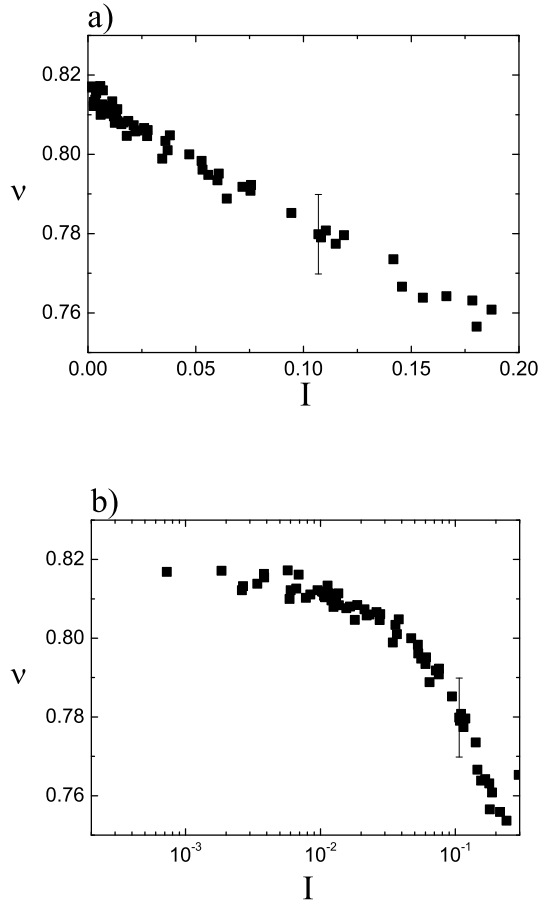


FIG. 3: Dilatancy law : (a) Linear scale (b) Logarithmic scale ( $\mu = 0.4$ , various  $e$  and  $\kappa$ ).

### B. Friction law

The effective friction coefficient has been defined as the ratio of the shear stress to the pressure inside the material  $\mu^* = S/P$ .

It could also be defined as the ratio of the (total) tangential and normal forces on the wall  $\mu_w^* = T/N$ . We have observed [26] that  $\mu_w^*$  is slightly larger than  $\mu^*$ . Some simulations have been carried out on to test the influence of the roughness, by taking glued grain on the wall twice as small ( $R = 0.5$ ) or twice as large ( $R = 2$ ) as the flowing grains, for the same  $I_g$ . This size ratio has an influence on the sliding velocity at the wall : it becomes noticeable for  $R = 0.5$  and decreases when  $R$  increases, since the grains close to the walls are trapped by the roughness. However, at distance from the walls, the flow remains homogeneous, but the shear rate, and hence  $I$ , decreases when  $R$  decreases. Furthermore, the effective friction at the wall decreases when  $R$  decreases. All in all,  $\mu_w^*(I)$  seems independent of  $R$ . For a more detailed dis-

cussion of the influence of the roughness on the flow (inclined plane and vertical chute), we refer to [25, 55, 60]. In the following we shall only discuss the effective friction coefficient in the volume of the flowing layer.

We call “friction law” the variations of the effective friction coefficient  $\mu^*$  (averaged over the width in the central part of the flowing layer) as a function of  $I$  (Fig. 4). We observe that  $\mu^*$  increases approximately linearly with  $I$ , starting from a minimum value  $\mu_{min}^*$  :

$$\mu^* \simeq \mu_{min}^* + bI, \quad (14)$$

with  $\mu_{min}^* \simeq 0.22$  and  $b \simeq 1.0$  (for  $\mu \neq 0$ ). The error bars (independent of  $I$ ) correspond to the statistical dispersion inside the layer. We also observe that  $\mu^*$  tends to saturate for  $I \geq 0.2$ . Within the error bars, it is difficult to be more precise about those dependencies. A more careful measurement is deferred for future work.

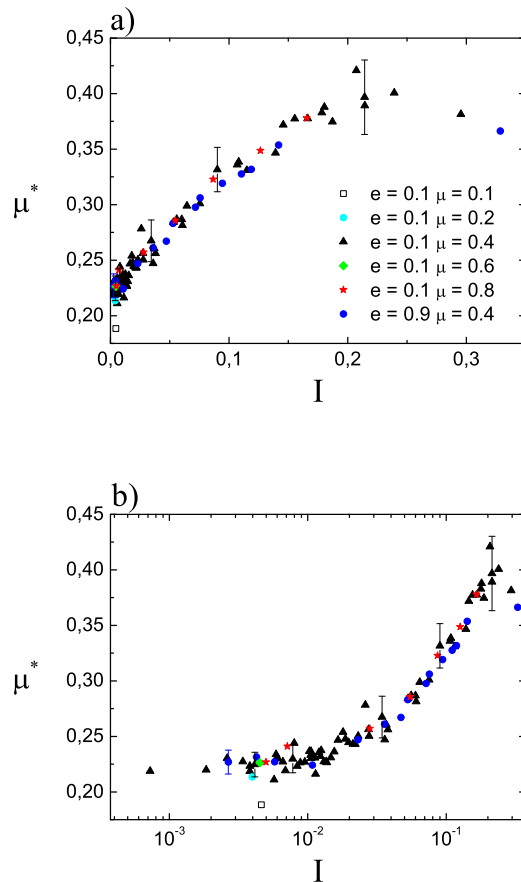


FIG. 4: (Color online) Friction law : (a) Linear scale (b) Logarithmic scale ( $\mu \neq 0$ , various  $e$  and  $\kappa$ ).

We now compare this friction law with other works. We first notice that the increase of  $\mu^*$  with  $I$  is contrary

to the well documented decrease of the friction coefficient with the velocity in the quasi-static regime [61]. However, in those studies, this softening is interpreted as a consequence of the renewal of the population of asperities at a microscopic scale, or as an effect of humidity [62]. Those effects do not come into play in our study. As a matter of fact, this friction law was already observed in previous discrete simulations [31], and partial observations (experimental or numerical) of the variation of  $\mu^*$  with the shear rate, the pressure or the solid fraction, consistent with our observations, may be found in [29, 35, 62, 63, 64, 65, 66, 67, 68]. Interestingly, the inclined plane geometry allows to prescribe both the effective friction and the pressure, through the inclination  $\theta$  of the plane and the height  $H$  of the flowing layer. Consequently, the measure of the superficial velocity  $V$  as a function of these two parameters provides a measure of the friction coefficient at the base as a function of  $I_g$  (which is proportional to  $V/H^{3/2}$ ) [69, 70]. Those observations are in good agreement with the previous friction law [26, 71].

### C. Comments

As a conclusion, in the limit of rigid grains, the classification of the flow regimes depends on the single dimensionless number  $I$ . In the quasi-static regime ( $I \leq 10^{-2}$ ), the granular material is very dense, close to the maximum solid fraction  $\nu_{max}$ , and the effective friction coefficient is close to its minimum value  $\mu_{min}^*$ . In the dynamic regime ( $I \geq 0.2$ ), the dilatancy becomes strong and the effective friction coefficient seems to saturate. The transition between those two regimes is progressive. In the intermediate regime ( $10^{-2} \leq I \leq 0.2$ ), we observe approximately linear variations of the solid fraction and of the effective friction coefficient as a function of  $I$  (Eqs. (13) and (14)).

In the case of a thin layer (see Sec. IV C), the dilatancy and friction laws are not affected. The parameters remain the same, except for the solid fraction which is smaller than for a thick layer :  $\nu_{max} = 0.82$  instead of 0.84 for  $\mu = 0$  and  $\nu_{max} = 0.78$  instead of 0.81 for  $\mu = 0.4$ .

In the case of a very small polydispersity (see Sec. IV D), the friction law is preserved in the central sheared layer. For larger polydispersity ( $\leq 50\%$ ), the dilatancy and friction laws are not affected.

When taking into account the elasticity of the grains, it is natural to draw a diagram of the flow regimes as a function of the two dimensionless numbers, already quoted in Sec. III B,  $\alpha = I/\sqrt{\kappa}$  and  $\nu$  [28, 39]. This leads to identify three regimes : elastic quasi-static, purely inertial and elastic-inertial. This last regime corresponds to very soft grains ( $\kappa < 100$ ) and is not accessible in our study, where we stay in the limit of rigid grains.

Furthermore, various studies where the volume rather than the pressure was prescribed [28, 34, 39, 53] have evidenced a transition between the quasi-static and the inertial regimes around a critical solid fraction. In our

study where the pressure is prescribed, the solid fraction adjusts to the inertial number  $I$ , so that the transition is not accessible.

### D. Constitutive law

We shall now show how these dilatancy and friction laws allow to deduce the constitutive law of the material, that is to say the dependencies of the pressure and shear stress on the shear rate and solid fraction :  $P(\nu, \dot{\gamma})$  and  $S(\nu, \dot{\gamma})$ .

#### 1. Pressure

From the definition of  $I$  (Eqn. (10)) and the dilatancy law (Eqn. (13)), the pressure may be expressed as a function of the shear rate and the solid fraction :

$$P(\nu, \dot{\gamma}) = \frac{a^2}{(\nu_{max} - \nu)^2} m \dot{\gamma}^2. \quad (15)$$

The divergency with the solid fraction is shown in Fig. 5.

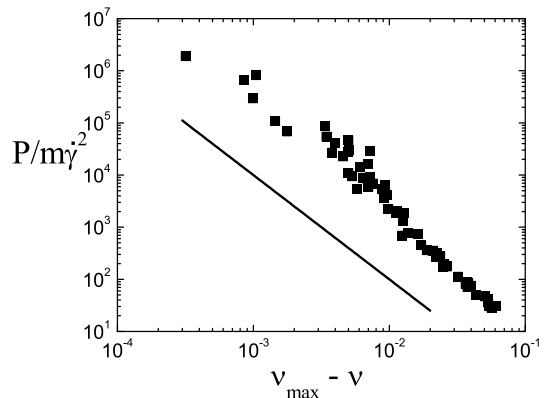


FIG. 5:  $P/\dot{\gamma}^2$  as a function of  $(\nu_{max} - \nu)$ . The straight line indicates a slope of  $-2$  ( $\mu = 0.4$ , various  $e$ ).

#### 2. Shear stress

From the definition of  $I$  (Eqn. (10)) and the friction law (Eqn. (14)), the shear stress may be expressed as a function of the shear rate and the pressure :

$$S(P, \dot{\gamma}) = \mu_{min}^* P + b\sqrt{mP}\dot{\gamma}. \quad (16)$$

Using the previous expression of  $P$  (Eqn. (15)), it is also possible to express the shear stress as a function of the shear rate and the solid fraction :

$$S(P, \nu, \dot{\gamma}) = \mu_{min}^* P + \frac{ab}{(\nu_{max} - \nu)} m \dot{\gamma}^2, \quad (17)$$

or, eliminating  $P$  :

$$S(\nu, \dot{\gamma}) = \frac{ab(\nu^* - \nu)}{(\nu_{max} - \nu)^2} m \dot{\gamma}^2, \quad (18)$$

with the solid fraction  $\nu^* = \nu_{max} + a\mu_{min}^*/b$  ( $\nu^* \approx 0.86$  for  $\mu = 0.4$ ).

### 3. Comments

We first notice that the dilatancy and friction laws, measured in the whole range of regimes, from the quasi-static to the dynamic, make the link between the known results in the two extreme regimes recalled in Sec. I. In the quasi-static regime,  $\mu_{min}^*$  and  $\nu_{max}$  may be identified with the internal friction  $\tan \phi$  and the critical solid fraction  $\nu_c$  in the critical state (see Sec IA).

In the intermediate regime ( $I < 0.2$ ), the expression of the stress components is analogous to the expression for a homogeneous system in the collisional regime (Eqs. (3)). The dependence on the square of the shear rate, similar to the original conclusions of Bagnold for concentrated suspensions [72], is a consequence of dimensional analysis [42]. The dependences on solid fraction are described by the following dimensionless functions :

$$\begin{cases} G_P(\nu) = \frac{a^2}{(\nu_{max} - \nu)^2}, \\ G_S(\nu) = \frac{ab(\nu^* - \nu)}{(\nu_{max} - \nu)^2}. \end{cases} \quad (19)$$

We recall (see Sec. IB) that the kinetic theory predicts a divergency in  $1/(1 - \nu)^2$  from the asymptotic behavior of the pair correlation function. However, when  $\nu \geq 0.67$  (so-called gel transition), then starts a regime of multiple collisions, strongly correlated, and the divergency rather seems in  $1/(\nu_{max} - \nu)$  [22, 40]. When the material is sheared, under the effect of cooperative rearrangements of caged grains, an even stronger divergency of the viscosity has been conjectured [73]. It seems that the precise form of these divergencies are decisive to describe the shape of the velocity profiles and for the jamming process [73, 74]. Our quantitative determination is then a precious information for the modelling of the dense granular flows.

We also notice that the expression (16) of  $S$  corresponds to a visco-plastic constitutive law, similar to the “frictional-collisional” decomposition of the stress tensor, with a contribution associated to maintained contacts, and a contribution associated to collisions [40, 75, 76, 77, 78]. In the viscous term, we notice that the apparent viscosity  $b\sqrt{mP}$  is proportional to the square root of

the pressure. The interpretation is that the typical momentum  $m\dot{\gamma}d$  is exchanged with the inertial time scale  $\sqrt{m/P}$  over a surface of the order  $d^2$ .

We think that the formulation of the constitutive law through the dilatancy and friction laws is simpler to use, since it avoids the treatment of divergency near jamming, which might be a problem in fluid mechanical numerical simulations.

## E. Influence of the mechanical parameters

We shall now describe the influence of the mechanical properties of the grains ( $k_n$ ,  $\mu$  and  $e$ ) on the dilatancy and friction laws.

### 1. Influence of the elasticity of the grains

In the limit of rigid grains, that is to say for  $\kappa \geq 10^4$ , we have not observed any influence of the stiffness coefficient  $k_n$  on the constitutive law. There is however an influence on the coordination number (see Sec. VII A). Furthermore, we have shown that softer grains favor localization of the shear (see Sec. IV D 2).

### 2. Influence of the local friction coefficient

The local friction coefficient  $\mu$  has a significant influence on the dilatancy law. The solid fraction remains a linearly decreasing function of  $I$ , but both parameters  $\nu_{max}$  and  $a$  depend on  $\mu$ .

The variation of  $a$  is not simple: we measure  $a = 0.38$  for  $\mu = 0$ ,  $0.31$  for  $\mu = 0.4$  and  $0.37$  for  $\mu = 0.8$  [26]. Fig. 6 (a) indicates that  $\nu_{max}$  is a decreasing function of  $\mu$  (it is not purely geometrical in the quasi-static regime). This shows that the solid fraction, from the critical state to the collisional regime, depends on the frictional properties of the material. We notice that our measurements are in agreement with other observations [34, 39, 79].

The influence of  $\mu$  on the friction law is less significant, except for frictionless grains ( $\mu = 0$ ). The Fig. 4, where  $\mu$  varies between 0.1 and 0.8, shows that  $\mu$  has nearly no influence on  $\mu^*$  in this range. This variation is more significant for small  $I$ . The Fig. 6 (b) shows more precisely the variation of the effective friction as a function of  $\mu$  in the quasi-static regime. There is strong variation between  $\mu = 0$  and  $\mu = 0.4$ , but above  $\mu = 0.4$  the effective friction remains constant.

As a conclusion, in the case of frictionless grains, the friction law keeps the same tendency but is shifted toward smaller values of friction (Fig. 7). However, we observe a saturation for  $I \geq 0.1$  if  $e = 0.9$ , which will be discussed in Sec. V E 4. For  $I \leq 0.1$ , the linear approximation (Eqn. (14)) is in trouble : it is rather a sub-linear dependency, and  $\mu_{min}^* \simeq 0.11$ . So the case of frictionless grains is singular and deserves a specific treatment.

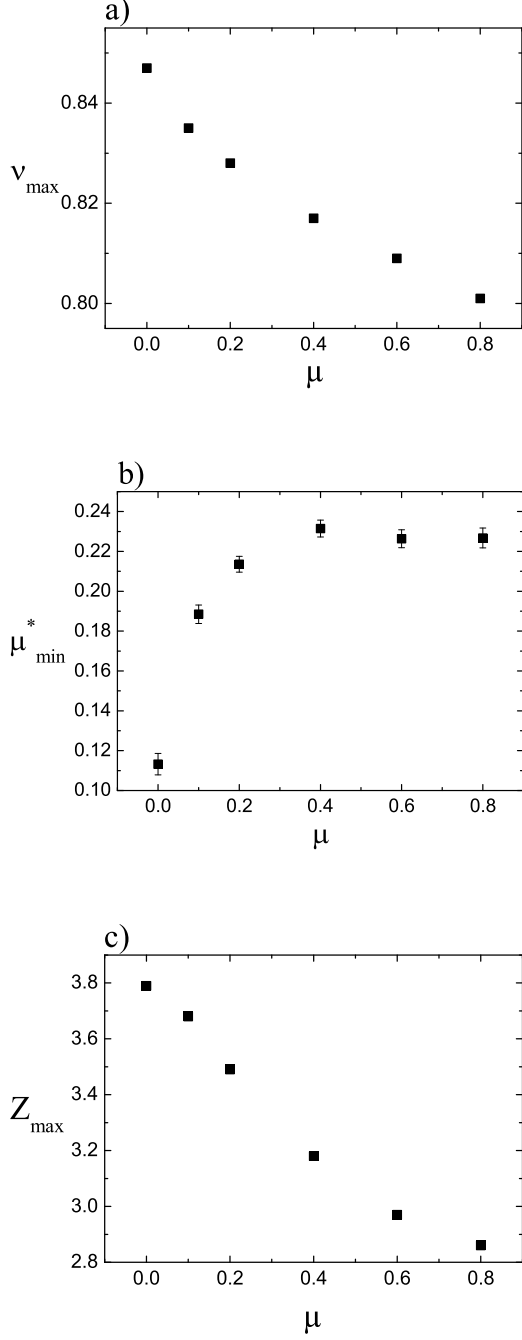


FIG. 6: Influence of  $\mu$  on the critical state ( $I = 4 \cdot 10^{-3}$  and  $e = 0.1$ ): (a) Maximum packing fraction  $\nu_{max}$ , (b) Effective friction coefficient  $\mu_{min}^*$ , (c) Coordination number  $Z_{max}$ .

Starting from both variations of solid fraction and effective friction as a function of the local friction coefficient  $\mu$ , it is tempting to draw the variations of the effective friction as a function of solid fraction instead of inertial number. This is done on Fig. 8. As a matter of

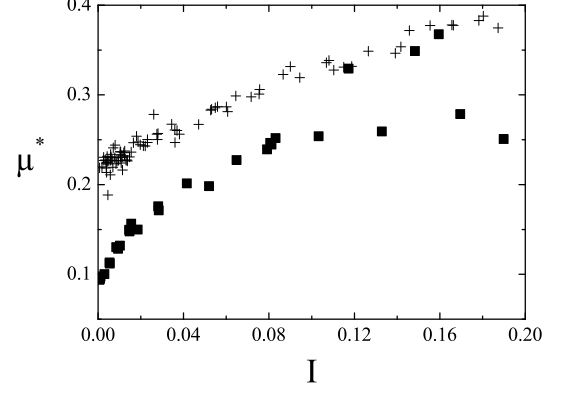


FIG. 7: Influence of  $\mu$  on the friction law ( $\mu = 0$  (■),  $\mu \neq 0$  (+)).

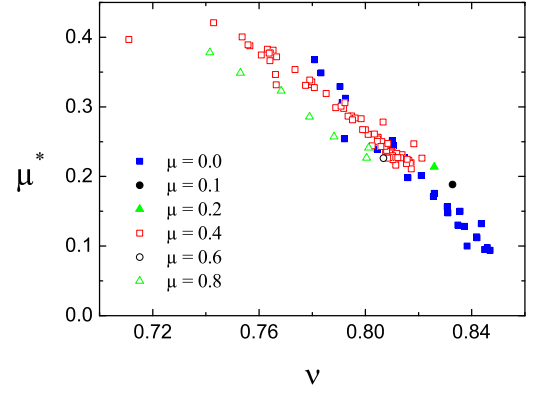


FIG. 8: (Color online) Variation of the effective friction coefficient as a function of solid fraction.

fact, Eqs. (15) and (18) predict :

$$\mu^*(\nu) = \frac{b}{a}(\nu^* - \nu), \quad (20)$$

where  $\nu^*$  was previously defined. This new representation of the results evidences a collapse of the data (even if  $a$ ,  $b$ ,  $\mu_{min}^*$  and  $\nu_{max}$  vary separately with  $\mu$ ,  $\nu^* = \nu_{max} + a\mu_{min}^*/b$  seems approximately constant). It appears that  $\mu^*$  becomes nearly independent of  $\mu$ . This master curve is made of complementary zones of high solid fraction for frictionless grains, and smaller solid fraction for frictional grains. It is noteworthy that a small variation of solid fraction (of the order of 10%) is enough to induce a variation of effective friction by a factor 4 ! This decrease of the effective friction when

the solid fraction increases is contrary to the observation in static compaction [80], but was previously observed under shear [65].

### 3. Influence of the restitution coefficient

The Fig. 4 shows that there is no influence of the restitution coefficient  $e$  for frictional grains. For frictionless grains, the comparison between slightly ( $e = 0.1$ ) and strongly ( $e = 0.9$ ) dissipative grains reveals (Fig. 9) that there is an influence, limited to the dynamic regime, for  $I \geq 0.1$ . Then, as the dissipation decreases, the dilatancy is less pronounced and the effective friction saturates (see also [39]).

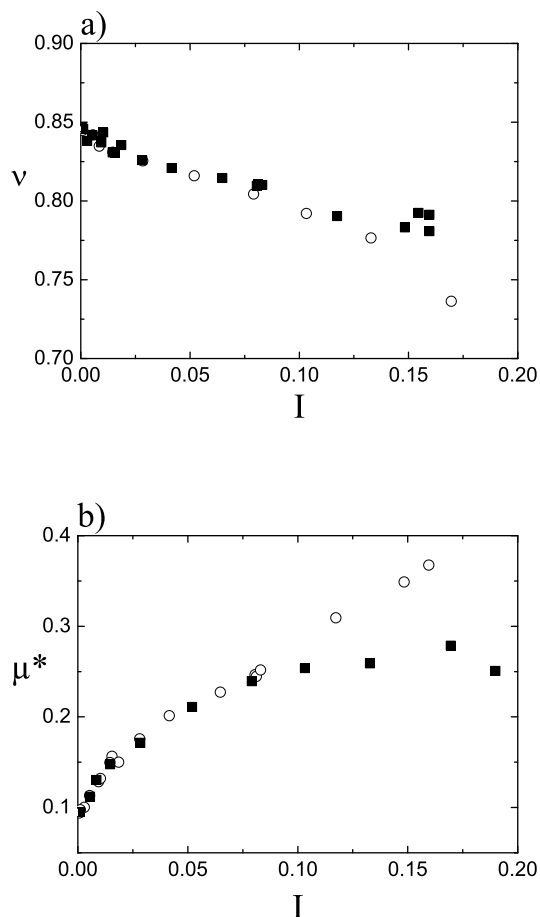


FIG. 9: Influence of  $e$  for  $\mu = 0$  ( $e = 0.9$  (■),  $e = 0.1$  (○)) : (a) Dilatancy law, (b) Friction law.

### 4. Collisional limit

The situation ( $I \geq 0.1$ ,  $\mu = 0$  and  $e = 0.9$ ) corresponds to the dense limit of the kinetic theory, with binary quasi-

elastic collisions (then the average contact time tends to the collision time [50]). In this dense limit, the Eqs. (3) predict a value of the effective friction independent of  $I$  but dependent on  $e$ , from the values of the pre-factors  $A_i$  [19] :

$$\mu^*(e) = \frac{\sqrt{A_S A_\Gamma}}{A_P} = \frac{1}{2} \left( \frac{\pi + 8}{2\pi} \right)^{\frac{1}{2}} \sqrt{1 - e^2}. \quad (21)$$

For  $e = 0.9$ , this predicts  $\mu^* = 0.29$  which is in fairly good agreement with the value measured for  $I = 0.2$  (0.26). The small difference between those two values may be due to the influence of the walls which induce a sliding velocity and gradients of the fluctuations [81].

## VI. FLUCTUATIONS

Up to now, all the quantities we have studied (solid fraction, velocities, forces) have been averaged in space and time. In fact, they are heterogeneous in space and fluctuate in time. The fluctuations of the forces have already been thoroughly studied [33, 34, 37, 53, 82]. We have observed [26] that the fluctuations of the forces are of the order of a few percents in the quasi-static regime, increase up to a factor 3 to 4 in the dynamic regime, and that they are larger near the walls than inside the sheared layer. We shall now discuss in detail the fluctuations of the motion of the grains.

### A. Intermittencies in the quasi-static regime

Various studies have shown that granular flows become unstable in the quasi-static regime. When the velocity is prescribed, one goes from a continuous flow regime to stick-slip [62, 83, 84]. When the shear stress is prescribed, one observes an hysteretic and abrupt fluid-solid transition [85]. We also notice that the observation of shear localization in discrete simulations of plane shear without gravity corresponds to the quasi-static regime [35, 38]. Space-time correlations of the motion of the grains have been observed [14, 23, 61, 86, 87, 88, 89]. Several rheological models have been proposed to describe those observations [25, 26, 40, 42, 90, 91, 92, 93, 94, 95]: transmission of forces at the scale of correlated clusters, two-phase fluid model with order parameter, activation of rearrangements through the fluctuations of velocity or forces.

Our study (see [26] for more details) shows that the flow is continuous in the intermediate regime, but becomes intermittent in the quasi-static regime (for  $I \leq I_0 \simeq 0.003$ ). Then the time averaged shear is homogeneous, but the instantaneous velocity profiles show that the layer oscillates between two states : a first one where the whole layer is at rest, caught to the fixed wall, except for a thin layer swept along by the moving wall, and a

second one where the whole layer is swept along by the moving wall except for a thin layer caught to the fixed wall. Those two extreme states have a very short duration, and the system is most of the time in an intermediate state, where the shear is approximately homogeneous in the whole layer. The pictures of the fields of velocity and velocity fluctuations show that the spatial correlations have a vortex like shape with a size between 3 and 4 grain diameter and are of a short duration. Consequently, the total kinetic energy fluctuates in time, with sudden peaks associated to the two extremal states, and slow variations associated to the intermediate situations. The Fig. 10 indicate that the relative fluctuations of the kinetic energy increase when  $I$  decreases and saturate in the quasi-static regime, according to :

$$\frac{\Delta E_c}{\langle E_c \rangle} \simeq \begin{cases} \frac{c}{I_0} & \text{for } I < I_0, \\ \frac{c}{I} & \text{for } I > I_0, \end{cases} \quad (22)$$

with  $I_0 \simeq 0.003$ .

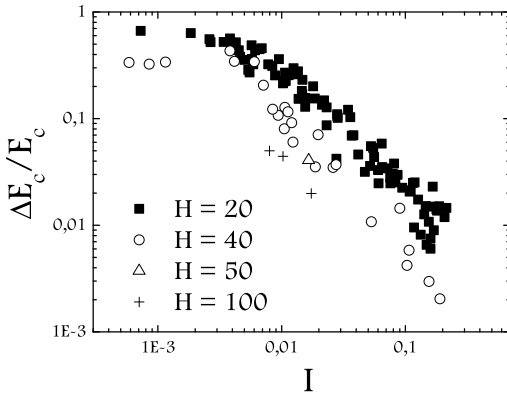


FIG. 10: *Relative fluctuations of the kinetic energy as a function of  $I$ . Influence of  $H$ .*

### B. Velocity fluctuations

We now discuss the fluctuations of the translation velocity  $\delta v$  and of the rotation velocity  $\delta \omega$  of the grains, which measure the agitation of the granular material. They are defined by :

$$\begin{cases} \delta v(y) = \sqrt{\langle \vec{v}(y)^2 \rangle - \langle \vec{v}(y) \rangle^2}, \\ \delta \omega(y) = \sqrt{\langle \omega(y)^2 \rangle - \langle \omega(y) \rangle^2}. \end{cases} \quad (23)$$

They are a natural variable in the description of collisional granular flows (see Sec. IB). Their influence is more difficult to analyze in the case of dense flows, where

the motions of the grains are strongly correlated [42]. The definition itself of those fluctuations is a problem, since it has been shown that they depend on the averaging time scale in the quasi-static regime [23]. Our analysis (long time scale) takes into account both the small fluctuations around the mean motion (in the “cage” formed by the nearest neighbors [96]), and the large fluctuations associated to collective motions in the quasi-static regime.

We notice that the quantities defined by Eqs. (23) are local, *i.e.* function of  $y$ . Those velocity fluctuations are uniform at the center of the sheared layer, but increase near the wall [26, 50]. According to various models, this agitation of the granular material near the rough walls is responsible for the increase of the shear rate (observed in Fig. 2 (b)) [42, 55, 73, 86, 97]. In the following, we consider the average velocity fluctuations in the central part of the sheared layer, excluding the 5 first layers near the walls.

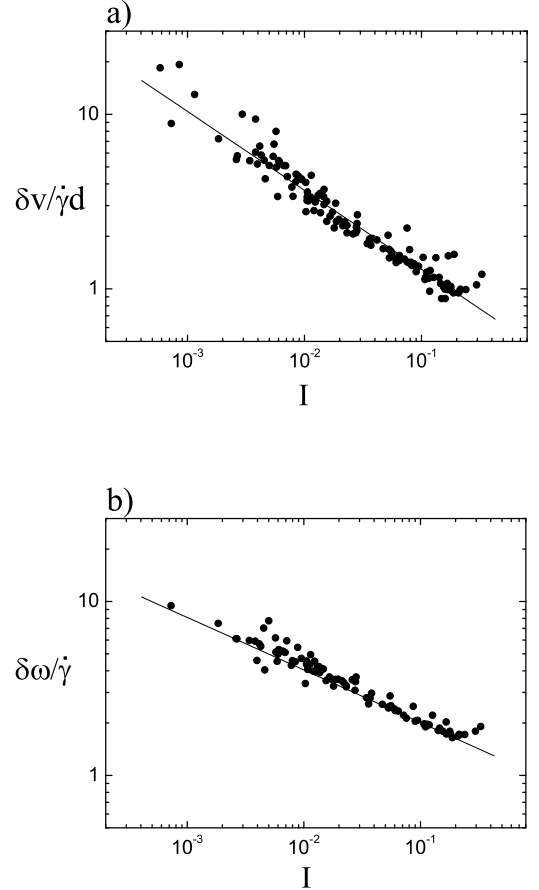


FIG. 11: *Relative velocity fluctuations as a function of  $I$  : (a) Translation velocity, (b) Rotation velocity (various parameters).*

Dimensional analysis suggests to analyze the variations

of the dimensionless quantities  $\delta v/\dot{\gamma}d$  and  $\delta\omega/\dot{\gamma}$  as functions of  $I$ . We consider  $\dot{\gamma}d$  as the natural scale of translation velocity, and  $\dot{\gamma}$  as the natural scale of rotation velocity (since  $\omega = -\frac{1}{2}\dot{\gamma}$ , see Sec. IV B 1). Those variations, drawn on Fig. 11, evidence two scaling laws, independent of the parameters of the system :

$$\begin{cases} \frac{\delta v}{\dot{\gamma}d} \simeq \frac{1}{3}I^{-\alpha}, \\ \frac{\delta\omega}{\dot{\gamma}} \simeq I^{-\beta}, \end{cases} \quad (24)$$

with  $\alpha \simeq \frac{1}{2}$  and  $\beta \simeq \frac{1}{3}$ , to which we shall refer as translation and rotation scaling laws.

The velocity fluctuations are significant (larger than 1) in the intermediate regime and very significant (larger than 10) in the quasi-static regime. In comparison, kinetic theory (see Eqs. (1) and (2)) predicts that  $\delta v/\dot{\gamma}d = \sqrt{A_s/A_\Gamma}$  that is to say  $\sqrt{\frac{\pi+8}{32(1-e^2)}} \simeq 1.3$ , for  $e = 0.9$ , which corresponds to the order of magnitude which is measured in the dynamic regime.

Large values of  $\delta\omega/\dot{\gamma}$  have been observed experimentally in the quasi-static regime [51] and in dense flows down inclined planes [55], and might be due to the frustration of the rotation [98].

We give two interpretations of the value of the exponent  $\alpha$ . The first explanation [25] consists in analyzing the motion of one grain as a succession of shear phases of duration  $1/\dot{\gamma}$  with a velocity  $\dot{\gamma}d$  and of sudden rearrangements with a velocity  $d\sqrt{P/m}$  of duration  $\sqrt{m/P}$ . This leads to  $\frac{\delta v}{\dot{\gamma}d} \simeq I^{-1/2}\frac{1-I}{1+I}$ . The second explanation relies on an energetic argument. In homogeneous shear, the work of the shear stress is balanced by the dissipation rate  $S\dot{\gamma} = \Gamma$ . If  $\Gamma$  describes the dissipation of the fluctuating kinetic energy  $m\delta v^2/2$  during the inertial time  $\sqrt{m/P}$ , we obtain :  $\delta v/\dot{\gamma}d \simeq \sqrt{2\mu^*(I)}I^{-1/2}$ . For both interpretations, the order of magnitude of the pre-factor is consistent with the observation.

We now show that the translation scaling law is consistent with the variations of the relative fluctuations of the kinetic energy (Eqn. (22)). Let us call  $\rho = \rho_g\nu$  the average solid fraction of the granular materials and  $\langle E_c \rangle$  the average kinetic energy by unit length, which is dominated by the translational part :  $\langle E_c \rangle = \frac{\rho}{2} \int_0^H (\dot{\gamma}y)^2 dy \sim (\rho V^2 H)$ . In the quasi-static regime, where the system oscillates between two localized flows,  $\Delta E_c \sim (\rho V^2 H)/2$ , so that  $\Delta E_c/\langle E_c \rangle \sim 1$ . In the dynamic regime,  $\Delta E_c \simeq \frac{\rho}{2} \int_0^H \delta v^2 dy$ . Using the translation scaling law for this last quantity, we get :  $\Delta E_c \sim \rho V^2/(HI)$ , so that  $\Delta E_c/\langle E_c \rangle \sim 1/(H^2I)$ . This is in agreement with the dependencies on  $I$  and  $H$  observed in Fig. 10.

Furthermore, the translation scaling law provides an estimation of the Reynolds contribution to the stress tensor (see Eqn. (12)) :  $\Sigma^f/\Sigma \simeq (2\nu/9\pi)I$ . This shows that in the intermediate regime ( $I \leq 0.1$ ), this contribution remains smaller than 1%, so that the contribution of the contact forces  $\Sigma^c$  remains dominant.

### C. Consequences for the constitutive law

The translation scaling law may also be written :

$$\frac{\delta v}{d} \simeq \frac{1}{3}\dot{\gamma}^{1/2}(P/m)^{1/4}. \quad (25)$$

Consequently, when the pressure is prescribed, the velocity fluctuations vary like  $\dot{\gamma}^{1/2}$ , instead of  $\dot{\gamma}$ . In the annular shear geometry, the pressure is constant along the radial direction, and an exponent close to 1/2 has been measured experimentally [73, 86].

If we introduce the velocity fluctuations in the constitutive law, like in the collisional regime (see Eqn. (1)), we obtain :

$$\begin{cases} P \simeq \frac{9a}{\nu_{max}-\nu}m(\delta v/d)^2, \\ S \simeq \frac{3b\sqrt{a}(\nu^*-\nu)}{(\nu_{max}-\nu)^{3/2}}m(\delta v/d)\dot{\gamma}. \end{cases} \quad (26)$$

Within this formulation, we notice a stronger divergence of the viscosity near the maximum solid fraction, like in the model inspired by the glassy dynamics [74].

## VII. CONTACT NETWORK

In addition to the macroscopic quantities which have been discussed, the discrete simulations provide information on the contact network. Its strongly heterogeneous character both in space and time has already been discussed in detail [28, 33, 34, 38, 45, 53, 54, 82, 97, 99, 100]: the contact time varies from the short collision time in the dynamic regime to the much longer shear time in the quasi-static regime [101], while the distribution of the force intensity is very wide. We shall not discuss in the following those distributions of contact time and force intensities. We shall rather focus on the following three quantities : coordination number, mobilization of friction and anisotropy of the contact forces.

### A. Coordination number

As was shown on Fig. 1, the contact network is very sensitive to the inertial number. A small dilation of the material (around 10%) is enough to observe a transition from a dense contact network to multiple, or even binary, collisions between grains. A quantitative indicator is the coordination number  $Z$ , that is to say the average number of contacts per grain. The variations of  $Z$  as a function of  $I$  are shown in Fig. 12.  $Z$  increases as  $I$  decreases, and tends toward a maximum value  $Z_{max}$  when  $I \rightarrow 0$ . A possible fit is:

$$Z = Z_{max} - cI^\gamma, \quad (27)$$

which is drawn on Fig. 12, which gathers the results for a given rigidity number  $\kappa$  and various  $e$  and  $\mu$ .

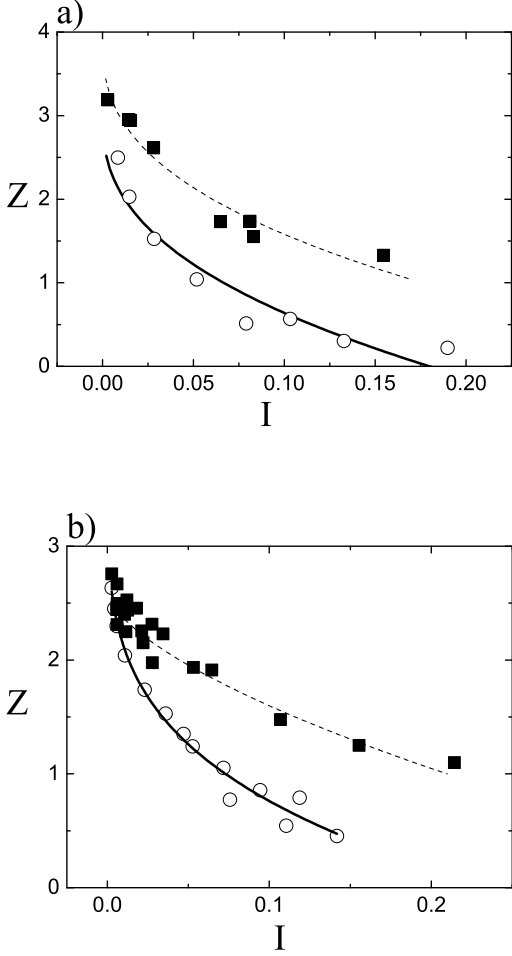


FIG. 12: Variation of the coordination number  $Z$  as a function of  $I$  ( $\kappa = 10^4$ ,  $e = 0.1$  (■),  $e = 0.9$  (○)) (a)  $\mu = 0$  - Fits  $Z = 3.75 - 7.11I^{0.51}$  (---),  $Z = 3.00 - 6.04I^{0.41}$  (-) (b)  $\mu = 0.4$  - Fits  $Z = 2.84 - 3.80I^{0.48}$  (---),  $Z = 2.60 - 5.48I^{0.50}$  (-).

Fig. 12 shows that the coordination number does not depend only on the geometry, through the solid fraction, but also on the mechanical properties of the grains  $e$  and  $\mu$ . The exponent  $\gamma$  is nearly constant ( $\gamma \simeq \frac{1}{2}$ ), but  $Z_{max}$  and  $c$  depend on  $e$  and  $\mu$ . When  $\mu$  decreases,  $Z$  increases and  $Z_{max}$  tends to 4 for frictionless grains [102] (see Fig. 6 (c)). We also notice that  $Z$  increases when  $e$  decreases, due to the increasing collision time. The Fig. 13 indicates that  $Z_{max}$  decreases significantly with  $\kappa$ , as expected. Among the various quantities which we have studied, the coordination number is the only one which varies significantly with the rigidity of the grains.

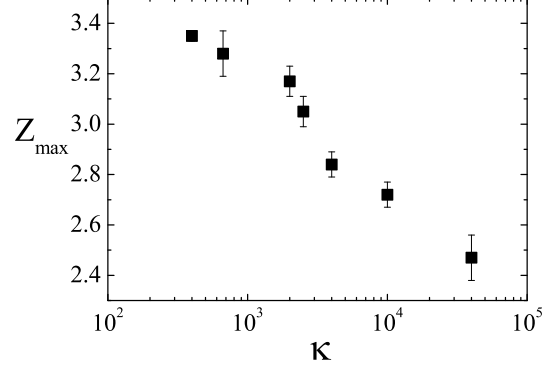


FIG. 13: Variation of the maximum coordination number as a function of  $\kappa$  ( $e = 0.1$ ,  $\mu = 0.4$ ).

## B. Mobilization of friction

Inside the population of contacts, and for frictional grains, we now introduce a distinction between the “sliding” contacts where the local friction is completely mobilized ( $|T| = \mu N$ ) and the other “rolling” contacts ( $|T| \leq \mu N$ ). This distinction is slightly different from the one proposed in [40], which distinguishes “fluid” contacts (collisions and sliding enduring contacts) and “solid” contacts (rolling enduring contacts). We define  $Z_s$  as the average number of sliding contacts per grain [103]. The Fig. 14 (a) shows the variations of  $Z_s$  as a function of the inertial number  $I$ . We observe that  $Z_s$  increases with  $I$  in the quasi-static regime, up to a maximum in the intermediate regime. Moreover, the Fig. 14 (a) indicates that the  $Z_s(I)$  curve depends on the restitution coefficient  $e$ .

We have shown on Fig. 14 (b) the variations with  $I$  of the ratio  $M = Z_s/Z$ , which, as the proportion of sliding contacts, is an indicator of the mobilization of friction. We observe that, contrarily to  $Z_s$ ,  $M$  increases, approximately logarithmically, as a function of  $I$ . We also notice a slight increase of  $M$  when  $\kappa$  increases.

## C. Anisotropy of the contact network

We now discuss the anisotropies of the contact network. We call  $\phi$  the direction of a contact counted counterclockwise from the  $x$  direction, between 0 and  $\pi$ .  $(\vec{n}_\phi, \vec{t}_\phi)$  is the local frame in the direction  $\phi$ . Let us call  $\langle N \rangle$  the average normal force in the homogeneous layer, then  $\langle N(\phi) \rangle$  and  $\langle T(\phi) \rangle$  the average normal and tangential forces in the homogeneous layer in the direction  $\phi$ . The anisotropies are described by the three angular distributions of contact orientations  $\rho(\phi)$ , of intensities of normal forces  $\xi_N(\phi) = \langle N(\phi) \rangle / \langle N \rangle$  and of intensities of tangential forces  $\xi_T(\phi) = \langle T(\phi) \rangle / \langle N \rangle$ . Then we define



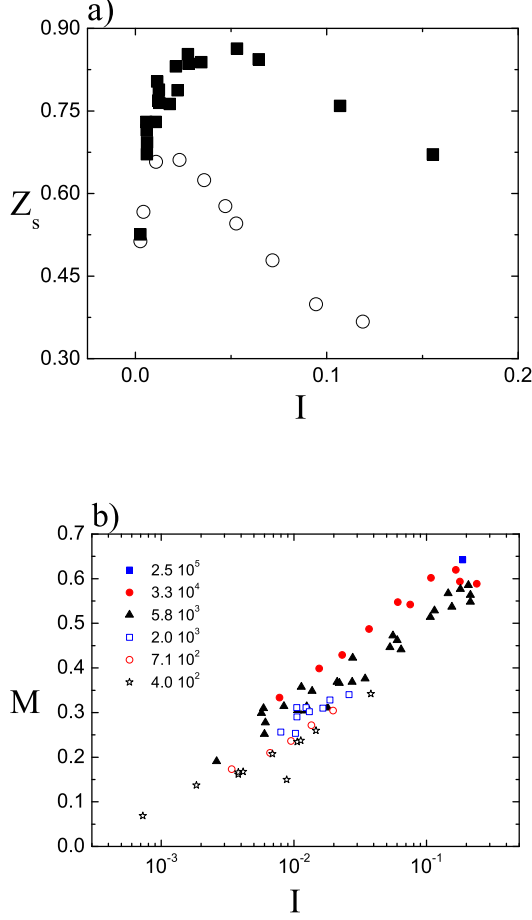


FIG. 14: (Color online) (a) Variation of  $Z_s$  as a function of  $I$  ( $\mu = 0.4$  -  $\kappa = 4000$  -  $e = 0.1$  (■),  $e = 0.9$  (○)) (b) Variation of  $M$  as a function of  $I$ , for various  $\kappa$ .

$\zeta_N(\phi) = \rho(\phi)\xi_N(\phi)$  and  $\zeta_T(\phi) = \rho(\phi)\xi_T(\phi)$ . Those angular distributions satisfy the normalization relations :

$$\begin{cases} \int_0^\pi \rho(\phi) d\phi = 1, \\ \int_0^\pi \zeta_N(\phi) d\phi = 1, \\ \int_0^\pi \zeta_T(\phi) d\phi = 0. \end{cases} \quad (28)$$

We show in Fig. 15 the two quantities  $\zeta_N(\phi)$  and  $\zeta_T(\phi)$  which will be useful in the discussion of the friction law. We distinguish first quasi-static and dynamic regimes, second frictional and frictionless grains. A positive value of  $\zeta_T(\phi)$  indicates that the tangential forces induce on average a counterclockwise rotation of the grains, and is represented with white symbols in Fig. 15 (c). A negative value of  $\zeta_T(\phi)$  indicates that the tangential forces induce on average a clockwise rotation of the grains, and is represented with black symbols in Fig. 15 (c).

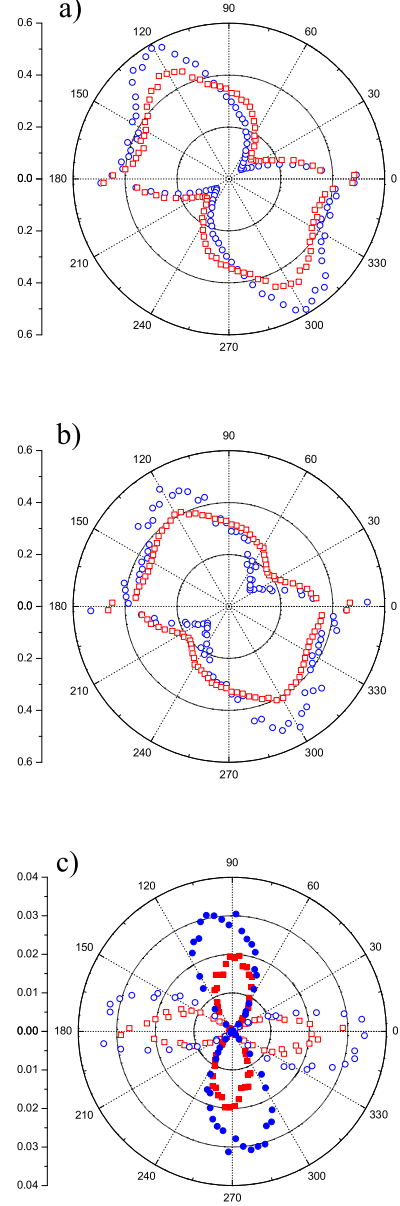


FIG. 15: (Color online) Angular distribution of the contact forces (quasi-static regime ( $I = 0.005$  - □), dynamic regime ( $I = 0.13$  - ○): (a)  $\zeta_N(\phi)$  ( $\mu = 0.4$ ), (b)  $\zeta_N(\phi)$  ( $\mu = 0$ ), (c)  $\zeta_T(\phi)$  ( $\mu = 0.4$ ) -  $\geq 0$  white symbols,  $\leq 0$  black symbols.

We notice a strong anisotropy of the contact network with privileged orientations for  $\zeta_N(\phi)$  along the directions of shear ( $\phi \simeq 0$  and  $\pi$ ) and of maximum compression ( $\phi \simeq 2\pi/3$ ), and for  $\zeta_T(\phi)$  along the directions of shear ( $\phi \simeq 0$  and  $\pi$ ) and of the shear gradient ( $\phi \simeq \pi/2$ ). Those anisotropies slightly change between the quasi-static and dynamic regimes and between frictional and frictionless grains cases.

Those anisotropies may be explained within a very sim-

plified picture of a granular material organized in layers along the shear direction. Then, there are two kinds of contacts between grains, inside a layer ( $\phi \simeq 0$  and  $\pi$ ) and between layers ( $\pi/3 \leq \phi \leq 2\pi/3$ ). The contacts between layers are created along the direction of maximum compression ( $\phi \simeq 2\pi/3$ ). In the quasi-static regime, those contacts are maintained up to the point where the grains separate ( $\phi \simeq \pi/3$ ). This is in contrast with the dynamic regime where the grains bounce, so that  $\zeta_N$  is stronger around  $\pi/3$  and smaller between  $\pi/3$  and  $2\pi/3$ .

We observe (see Fig. 16 (a)) that the tangential anisotropy is well described by the following expression :

$$\zeta_T(\phi) = f_T(I)\zeta_N(\phi) \cos(2\phi), \quad (29)$$

with an increasing positive function  $f_T(I)$ . This means that the contacts between layers favor a clockwise rotation of the grains, while the contacts inside layers favor a counterclockwise rotation of the grains. Furthermore, this shows that the average tangential force is smaller in the quasi-static regime than in the dynamic regime.

## VIII. MICROSCOPIC ORIGIN OF THE FRICTION LAW

We now try to understand quantitatively the macroscopic friction law on the basis of the previous microscopic information (fluctuations and anisotropy of the contact network).

### A. Friction and rotation

We first discuss the tangential anisotropy and show how it is related to the rotation of the grains [98].

#### 1. Average rotation

In a first step, we take into account the average rotation velocity  $\omega$ . We consider the homogeneous shear of an assembly of grains of diameter  $d$  with an average shear rate  $\dot{\gamma}$ . Then, the tangential relative velocity between two grains (see Sec. II B) is given by :

$$V^T(\phi) = d(\omega + \dot{\gamma} \sin^2(\phi)). \quad (30)$$

The average tangential force exerted on a grain should be equal to zero in steady state :

$$\int_0^\pi \rho(\phi)T(\phi)d\phi = 0. \quad (31)$$

We start with two very crude assumptions : all the contacts are sliding ( $T = -\mu N \text{sign}(V^T)$ ) and the normal

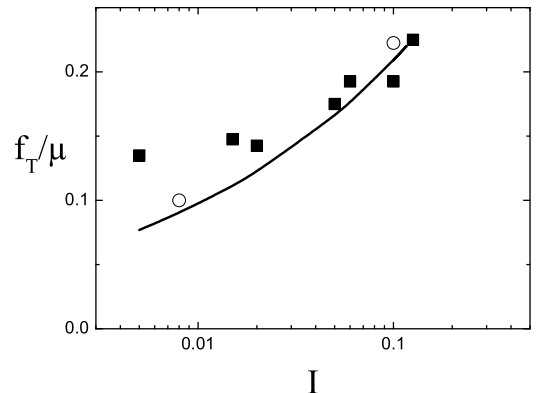
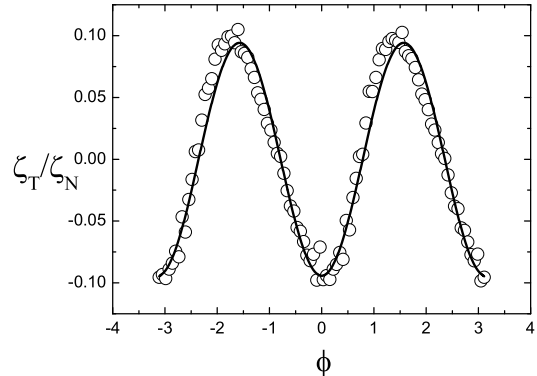


FIG. 16: Angular distribution of tangential contact forces: (a)  $\zeta_T(\phi)/\zeta_N(\phi)$  ( $\circ$ ) fitted by  $f_T \cos(2\phi)$  (—) for  $I = 0.13$  and  $\mu = 0.4$ , (b)  $f_T(I)/\mu$  for  $\mu = 0.4$  ( $\blacksquare$ ) and  $\mu = 0.8$  ( $\circ$ ) compared with  $\frac{\sqrt{2}}{\pi} I^{1/3}$ .

force distribution is isotropic ( $\zeta_N(\phi) = 1/\pi$ ). Consequently :

$$\int_0^\pi \text{sign}(\omega + \dot{\gamma} \sin^2(\phi))d\phi = 0. \quad (32)$$

This is an explanation for the relation  $\omega = -\frac{1}{2}\dot{\gamma}$ , which was described in Sec. IV B 1 (see Fig. 2 (b)). Consequently  $V^T(\phi) = -d\dot{\gamma} \cos(2\phi)/2$ ,  $\zeta_T = \mu/\pi$  when  $0 \leq \phi \leq \pi/4$  and  $3\pi/4 \leq \phi \leq \pi$  and  $\zeta_T = -\mu/\pi$  when  $\pi/4 \leq \phi \leq 3\pi/4$ . In comparison with Fig. 15 (c), we notice that the sign of  $\zeta_T(\phi)$  is correct, but that the order of magnitude is too large, by a factor of around 10.

#### 2. Fluctuations of the rotation

As a way to understand the order of magnitude of  $\zeta_T(\phi)$ , we now take into account the fluctuations of the

rotation velocity, which have been evidenced in Sec. VI. Denoting as  $\delta\omega_{i,j}$  the fluctuations of rotation of two grains  $i$  and  $j$  in contact, their relative tangential velocity at the contact point becomes :

$$V_{ij}^T(\phi) = -d\dot{\gamma} \cos(2\phi)/2 + d/2(\delta\omega_i + \delta\omega_j). \quad (33)$$

Keeping the assumption of sliding contacts, we predict :

$$\zeta_T(\phi) = -\mu\zeta_N(\phi)\langle \text{sign}(V^T) \rangle, \quad (34)$$

where  $\langle \text{sign}(V^T) \rangle$  is the statistical average over the fluctuating rotations of the two grains. Discrete numerical simulations have shown that the distribution of the rotation velocity is approximately lorentzian [55]. We make the assumption that the fluctuations of rotation of two grains in contact are not correlated. Then the random variable  $(\delta\omega_i + \delta\omega_j)/2$  follows a lorentzian distribution, with a zero mean value and a variance  $\delta\omega/\sqrt{2}$ . Then we obtain :

$$\langle \text{sign}(V^T) \rangle = -\frac{2}{\pi} \arctan\left(\frac{\dot{\gamma}}{\sqrt{2}\delta\omega} \cos(2\phi)\right). \quad (35)$$

Using the rotation scaling law (24) :

$$\langle \text{sign}(V^T) \rangle = -\frac{2}{\pi} \arctan\left(\frac{I^{1/3}}{\sqrt{2}} \cos(2\phi)\right), \quad (36)$$

and for small  $I$  ( $\leq 0.2$ ) :

$$\langle \text{sign}(V^T) \rangle \simeq -\frac{\sqrt{2}}{\pi} I^{1/3} \cos(2\phi), \quad (37)$$

so that at the end :

$$\zeta_T(\phi) \simeq \frac{\sqrt{2}}{\pi} \mu I^{1/3} \zeta_N(\phi) \cos(2\phi). \quad (38)$$

This expression reproduces the observed angular dependence in  $\zeta_N(\phi) \cos(2\phi)$ , shown in Fig. 16 (a). The prediction for the dependence of the amplitude on  $I$  and  $\mu$  is in agreement with the observed pre-factor  $f_T(I)$  defined in Eqn. (29), as shown in Fig. 16 (b). The order of magnitude is now consistent with the observations.

As a conclusion, the fluctuations of the rotation velocity are a possible quantitative explanation of the angular distribution of tangential forces  $\zeta_T(\phi)$ . When  $I$  decreases, the relative fluctuations of rotation increase, so that the average relative tangential velocity of two grains in contact tends to zero, which kills the frictional effect. This model is very crude. In the dynamic collisional regime, we have seen that most of the contacts are sliding (see Fig. 14) and the assumption of uncorrelated fluctuations may seem reasonable. On the contrary, in the

quasi-static regime, we have observed that most of the contacts are rolling. Furthermore, our simulations reveal correlations of the rotations of grains in contact: it seems that the flowing granular material is organized in clusters of grains rotating in the same way [98]. Such correlations of the grain motion deserves further study [89, 95].

## B. Friction and anisotropy

We now discuss the friction law  $\mu^*(I)$  on the basis of the information on the contact network. We would like to understand the increase of  $\mu^*$  with  $I$ , and its dependence with the microscopic friction  $\mu$ .

A first possible interpretation lies in the increase of the mobilization of friction  $M(I)$  (Fig. 14 (b)): most of the contacts are rolling in the quasi-static regime, while most of them are inelastic sliding collisions in the dynamic regime. Consequently, the energy dissipation, and hence the effective friction, should be stronger in the dynamic regime. However, since the effective friction coefficient of an assembly of frictionless grains is not equal to zero, this interpretation is certainly not sufficient. We are now going to show the crucial role of the anisotropies of the contact network.

We consider the homogeneous shear of an assembly of grains of diameter  $d$  with average solid fraction  $\nu$ , coordination number  $Z$ , and normal force  $\langle N \rangle$ . The stress tensor is dominated by the contribution of the contacts (see Eqn. 12). It is possible to express it as a function of the angular distributions of contact forces, which we have previously defined [51, 55, 104, 105]:

$$\underline{\underline{\Sigma}} = \frac{2\nu Z \langle N \rangle}{\pi d} \int_0^\pi [\zeta_N(\phi) \vec{n}_\phi + \zeta_T(\phi) \vec{t}_\phi] \otimes \vec{n}_\phi d\phi. \quad (39)$$

Using the properties of the stress tensor ( $\Sigma_{xy} = \Sigma_{yx}$ , and  $\Sigma_{xx} = \Sigma_{yy}$ ) and the normalization of angular distributions, the effective friction coefficient takes the simple expression :

$$\mu^* = - \int_0^\pi [\zeta_N(\phi) \sin(2\phi) + \zeta_T(\phi) \cos(2\phi)] d\phi. \quad (40)$$

In the first term associated to the normal forces ( $\mu_N^*$ ), the factor  $\sin(2\phi)$  is positive for  $\phi$  between 0 and  $\pi/2$ , so that it decreases the effective friction, and negative for  $\phi$  between  $\pi/2$  and  $\pi$ , so that it increases the effective friction. Consequently, the evolution of the angular distribution between the quasi-static regime and the dynamic regime (see Fig. 15 (a) and (b)) might explain part of the increase of the effective friction.

It is possible to give an estimation of the second term associated to the tangential forces ( $\mu_T^*$ ), using the approximation (38) for  $\zeta_T(\phi)$ , with  $\zeta_N(\phi) = 1/\pi$ . We obtain  $\mu_T^* \simeq -(\mu/\sqrt{2}\pi) I^{1/3}$ . This contribution is negative and small. The complete calculation (Fig. 17 (b)) confirms that the contribution of tangential forces to the

effective friction ( $|\mu_T^*|/\mu^*$ ) remains of the order of 15% for  $\mu = 0.4$  and 30% for  $\mu = 0.8$ .

Fig. 17 (a) compares the prediction based on the angular distribution (40) with the complete calculation based on (12), both for frictional and frictionless grains (the results of Fig. 7). The agreement is very good for frictionless grains, but we observe a deviation for frictional grains, of the order of 15%, which we do not explain at this stage. A possible explanation is the small polydispersity since the monodispersity was the only simplifying assumptions leading to (40).

This result is very paradoxical. Contrarily to our first tentative explanation of the friction law, rather than explaining the macroscopic friction, the microscopic friction (tangential forces) has a small and even negative contribution to the macroscopic friction. The friction law depends mostly on the angular distribution of normal forces. A small variation of the distribution is enough to increase the effective friction by a factor of two between the quasi-static and the dynamic regime. In the same way, this distribution is more isotropic in the case of frictionless grains, and this explains the shift of the friction law. The microscopic friction has an indirect effect on the friction law, through the modification of the angular distribution of normal forces. This would mean that the very origin of the visco-plastic constitutive law relies in the anisotropy of the contact network (fabric) in response to the shear. This point which has already been studied in the quasi-static regime [13] would deserve further study.

## IX. INFLUENCE OF GRAVITY

Up to now, we have studied the simplest flow geometry, plane shear between two rough walls, without gravity. Then the stress distribution is homogeneous. In the limit of rigid grains and in the intermediate regime, we have observed steady homogeneous flows, in which we have measured the dilatancy and friction laws. Other simulations of homogeneous shear states without walls have confirmed those observations [106].

We now wonder if those laws are valid in other flow geometries (annular shear, vertical chute, inclined plane...) where, as a consequence of the heterogeneous stress distribution, the flow is no more homogeneous, and often localized near the walls or the free surface [25, 26].

As a simple example of an heterogeneous stress distribution, we still consider the plane shear flow geometry, but we study the influence of gravity  $g$  along  $y$  (oriented toward the fixed wall). Then, the shear stress  $S$  remains constant in the sheared layer, but the pressure varies along  $y$  according to :

$$P(y) = P_w + \rho_g g \int_y^H \nu(t) dt. \quad (41)$$

where  $P_w$  is the pressure prescribed on the moving wall.

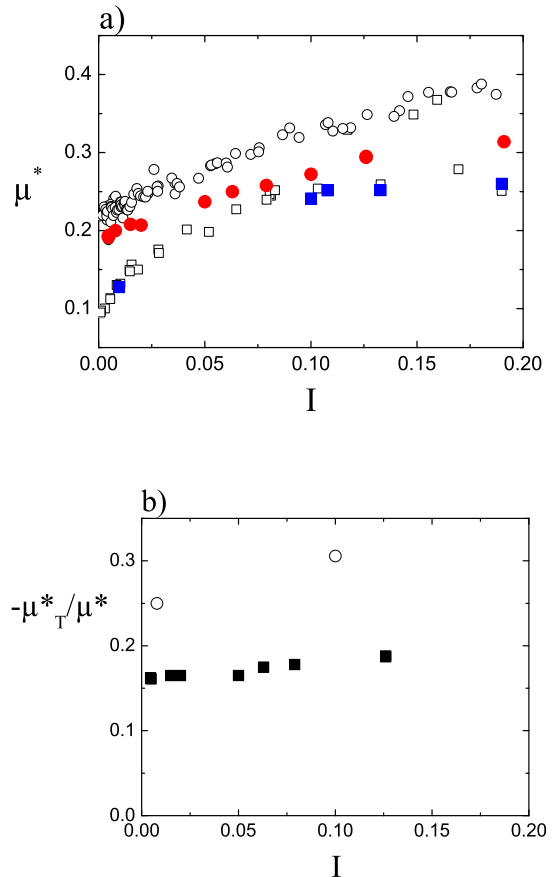


FIG. 17: (Color online) Friction and anisotropy : (a) Comparison of Eqn. 40 (black symbols) with direct measurement of Fig. 7 (open symbols) ( $\mu = 0$  ( $\square$ ),  $\mu \neq 0$  ( $\circ$ )), (b) Tangential contribution for  $\mu = 0.4$  ( $\blacksquare$ ) and  $\mu = 0.8$  ( $\circ$ ).

We notice that this kind of flow has been previously studied experimentally [63, 64, 65, 83, 107], numerically [29, 30, 37, 40] and theoretically [75].

### A. Dimensional analysis

We define dimensionless numbers from the various time scales of the system, and notice that in an heterogeneous system, those quantities depend on  $y$ . In addition to the shear time  $1/\dot{\gamma}(y)$ , the inertial time  $\sqrt{m/P(y)}$ , and the collision time  $\tau_c$ , the presence of gravity introduces another gravity timescale  $\sqrt{d/g}$ . Consequently, in addition to the inertial  $I(y)$  and rigidity  $\kappa(y)$  numbers, we must consider a third dimensionless number, measuring the intensity of gravity. We call  $G(y)$  this gravity number,

defined as the ratio of inertial to gravity times :

$$G(y) = \sqrt{\frac{gm}{P(y)d}}. \quad (42)$$

In the following, we have not studied the influence of the rigidity of the grains :  $\kappa(y)$  varies between  $10^4$  near the moving wall and  $10^2$  near the fixed wall, where we are beyond the rigid grain limit. The simulated systems ( $H/d \simeq 40$ ) are described by the two dimensionless numbers  $I_g = V/H\sqrt{m/P_w}$  and  $G = \sqrt{\frac{gm}{P_w d}}$ .  $I_g$  varies between 0.0025 and 0.05, whereas  $G$  varies between 0 and 3.2.

### B. Localization

Let us first assume that the dilatancy and friction law identified in homogeneous shear flows are still valid in presence of gravity. Then we predict that, like  $S/P(y)$ ,  $I(y)$  should decrease from  $y = H$  to  $y = 0$ . Consequently the shear rate should decrease and the solid fraction increase. For a large enough  $G$ , there is a point  $(H - \lambda)$  where  $S/P(H - \lambda) = \mu_{min}^*$ . Below this point, the granular material should be at rest:  $\dot{\gamma} = 0$  and  $\nu = \nu_{max}$ . This would mean that the shear is localized in a layer of width  $\lambda$ .

The measured velocity profiles  $v_x(y)$  (Fig. 18 (a)) indicate a shear localization near the moving wall. Those profiles are approximately exponential in the upper part (see [40]),  $v_x(y) \simeq V \exp(-\frac{H-y}{\lambda})$ , from which we estimate the width of the shear layer  $\lambda$ . Contrarily to the annular shear or vertical chute geometries [25], where this length is always of the order of five to ten grain diameters, this length strongly varies as a function of  $G$  (Fig. 18 (b)) and diverges when  $G \rightarrow 0$ , which means that the flow becomes homogeneous in the limit of small gravity. The solid fraction increase at distance from the moving wall and is very high in the quasi-static region.

### C. Dilatancy and friction laws

For each value of  $G$ , we deduce from  $\nu(y)$ ,  $\dot{\gamma}(y)$ ,  $P(y)$  and  $S(y)$  the variations of the local solid fraction and of the effective friction coefficient as a function of the local inertial number (Fig. 19 (a) et (b)). A single simulation provides the whole curve, but the data are noisy since they result from local measurements, which are not averaged over the whole layer. The tendency is analogous to the no-gravity case: decrease of  $\nu$  from  $\nu_{max}$ , and increase of  $\mu^*$  from  $\mu_{min}^*$  when  $I$  increases. However, as  $G$  increases,  $\nu_{max}$  increases while  $\mu_{min}^*$  decreases. The  $a$  and  $b$  factors are affected as well.

We have also measured the influence of  $G$  on the contact network and on the fluctuations [26] :  $G$  has nearly no influence on the  $Z(I)$  and  $M(I)$  dependencies; the

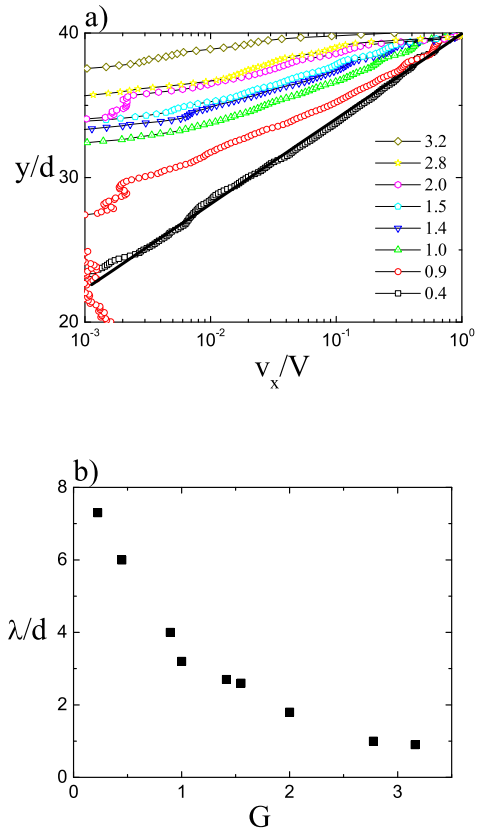


FIG. 18: (Color online) Influence of  $G$ : (a) Velocity profiles (logarithmic scale) (b) Width  $\lambda$  of the shear layer ( $H/d = 40$ ,  $e = 0.1$ ,  $\mu = 0.4$ ,  $I_g = 0.015$ )

translation and rotation scaling laws (24) remain valid but the exponents  $\alpha$  and  $\beta$  increase respectively from 0.5 to 0.6 and from 0.3 to 0.5.

### D. Comments

Those measurements indicate that the measurements performed in homogeneous shear flows are not sufficient to describe other flow geometries. Then, the inertial number is not the only relevant quantity to describe the shear flow. We must take into account other quantities, such as the gravity number in plane shear flows with gravity. At this stage, we are not able to explain quantitatively the observations which we have briefly quoted, such as the nearly exponential shear localization, or the decrease of  $\mu_{min}^*$  with  $G$ . Following our explanation of the friction law in the homogeneous case (see Sec. VIII), we suggest that this could be related to the evolution of the anisotropy of the contact network: as  $G$  increases, the distribution  $\zeta_N(\phi)$  would increase for  $0 \leq \phi \leq \pi/2$ .

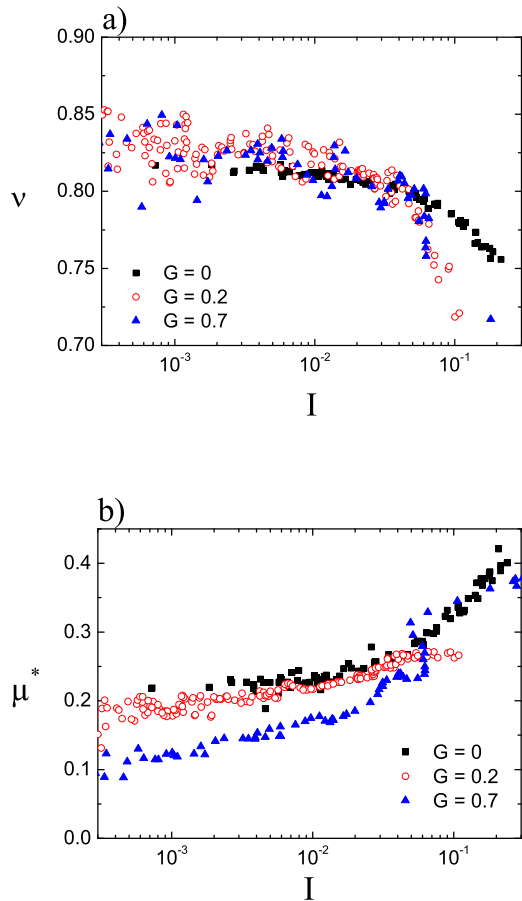


FIG. 19: (Color online) Influence of  $G$ : (a) Dilatancy law (b) Friction law (logarithmic scale) ( $e = 0.1, \mu = 0.4, I_g = 0.015$ ).

## X. CONCLUSION

We now summarize our conclusions. We have considered the simplest flow geometry (plane shear without gravity), where the stress distribution is homogeneous. Using molecular dynamics simulation, we have submitted a dense assembly of frictional, inelastic disks, to a given pressure and shear rate. We have observed steady homogeneous shear flows, which become intermittent in the quasi-static regime. We have shown that, in the limit of rigid grains, the shear state is determined by a single dimensionless number, called inertial number  $I$ , which describes the ratio of inertial to pressure forces. Small

values of  $I$  correspond to the quasi-static critical state regime of soil mechanics, while large values of  $I$  correspond to the dynamic collisional regime of the kinetic theory. When  $I$  increases in the intermediate regime, we have measured an approximately linear decrease of the solid fraction from the maximum packing value, and an approximately linear increase of the effective friction coefficient from the static internal friction value. From those dilatancy and friction laws, we have deduced a visco-plastic constitutive law, with a plastic Coulomb term and a viscous Bagnold term. We have also measured scaling laws for the relative velocity fluctuations as a function of  $I$ . We have shown that the mechanical characteristics of the grains (restitution, friction and elasticity) have a very small influence in the intermediate regime. We have shown that the origin of the friction law relies in the fluctuating rotations of the grains and on the angular distribution of contact forces.

The study of plane shear flows with gravity has shown that the generalization to other heterogeneous flow geometries is not straightforward. However, the study of annular shear flows [26] and inclined plane flows [26, 42, 71] reveal the same qualitative tendencies. Other flow geometries such as vertical chute, rotating drum and heap flow should be analyzed in the same way [25].

We notice that a generalization of those ideas to steady uniform shear flows of cohesive granular materials has been successful [106].

In this paper, we have restricted our attention to velocity controlled shear flows, so that it was not possible to study the flow threshold. We think that it was evidenced indirectly through the appearance of intermitencies for small enough  $I$  [95]. A specific study of the jamming mechanisms should be performed by controlling the shear stress, either in plane shear flows [40] or down inclined planes [26, 71].

## Acknowledgments

We gratefully acknowledge Lydéric Bocquet, Philippe Coussot, Ivan Iordanoff, Jim Jenkins, Pierre Mills and Olivier Pouliquen for many interesting discussions at various stages of this study.

Laboratoire des Matériaux et Structures du Génie Civil is a joint laboratory, depending on Laboratoire Central des Ponts et Chaussées, Ecole Nationale des Ponts et Chaussées and Centre National de la Recherche Scientifique.

- 
- [1] K. R. Hutter and K. R. Rajagopal, *Cont. Mech. Thermodyn.* **6**, 81 (1994).  
 [2] P. Coussot and C. Ancey, *Rhéophysique des pâtes et des suspensions* (EDP Sciences, Orsay, 1999).

- [3] J. Rajchenbach, *Adv. in Physics* **49**, 229 (2000).  
 [4] H. Hinrichsen and D. Wolf (Wiley-Vch, Weinheim, 2004).  
 [5] R. Jackson, in *Theory of dispersed multiphase flow*,

- edited by R. Meyer (Academic Press, New York, 1983), pp. 291–337.
- [6] R. Nedderman, *Statics and kinematics of granular materials* (Cambridge University Press, Cambridge, 1992).
- [7] P. A. Vermeer, in *Physics of dry granular media*, edited by H. J. Hermann, J. P. Hovi, and S. Luding (Balkema, Dordrecht, 1998), pp. 163–196.
- [8] G. Tardos, *Powder Tech.* **92**, 61 (1997).
- [9] G. Gudehus, F. Darve, and I. Vardoulakis, eds., *Constitutive Relations for Soils* (Balkema, Rotterdam, 1984).
- [10] W. Wu, E. Bauer, and D. Kolymbas, *Mechanics of Materials* **23**, 45 (1996).
- [11] A. N. Schofield and C. P. Wroth, *Critical state soil mechanics* (McGraw-Hill, London, 1968).
- [12] D. M. Wood, *Soil Behaviour and Critical State Soil Mechanics* (Cambridge University Press, 1990).
- [13] F. Radjai and S. Roux, in *The physics of granular media*, edited by H. Hinrichsen and D. Wolf (Wiley-Vch, Weinheim, 2004).
- [14] J. N. Roux and G. Combe, *Comptes Rendus Physique* **3**, 131 (2002).
- [15] G. Combe and J.-N. Roux, in *Deformation characteristics of geomaterials*, edited by H. di Benedetto, T. Doanh, H. Geoffroy, and C. Sauzéat (Swets and Zeitlinger, Lisse, 2003), pp. 1071–1078.
- [16] S. Roux and F. Radjai, *Physics of Dry Granular Media* (Kluwer Academic, Dordrecht, 1998), chap. Texture-dependent rigid-plastic behaviour, pp. 229–235.
- [17] P. K. Haff, *J. Fluid Mech.* **134**, 401 (1983).
- [18] J. T. Jenkins and S. B. Savage, *J. Fluid Mech.* **130**, 187 (1983).
- [19] J. T. Jenkins and M. W. Richman, *Phys. Fluids* **28**, 3485 (1985).
- [20] C. S. Campbell, *Annu. Rev. Fluid Mech.* **22**, 57 (1990).
- [21] I. Goldhirsch, *Chaos* **9**, 659 (1999).
- [22] S. Luding, *Phys. Rev. E* **63**, 042201 (2001).
- [23] F. Radjai and S. Roux, *Phys. Rev. Lett.* **89**, 064302 (2002).
- [24] O. Pouliquen and F. Chevoir, *Comptes Rendus Physique* **3**, 163 (2002).
- [25] GDR MIDI, *Euro. Phys. J. E* **14**, 341 (2004).
- [26] F. da Cruz, Ph.D. thesis, Ecole Nationale des Ponts et Chaussées (2004), in French.
- [27] P. A. Cundall, *Ingenieur Archiv* **59**, 148 (1989).
- [28] M. Babic, H. H. Shen, and H. T. Shen, *J. Fluid Mech.* **219**, 81 (1990).
- [29] P. A. Thompson and G. S. Grest, *Phys. Rev. Lett.* **67**, 1751 (1991).
- [30] Y. Zhang and C. S. Campbell, *J. Fluid Mech.* **237**, 541 (1992).
- [31] J. D. Dent, *Annals Glaciology* **18**, 215 (1993).
- [32] C. K. K. Lun and A. A. Bent, *J. Fluid Mech.* **258**, 335 (1994).
- [33] O. J. Schwarz, Y. Horie, and M. Shearer, *Phys. Rev. E* **57**, 2053 (1998).
- [34] E. Aharonov and D. Sparks, *Phys. Rev. E* **60**, 6890 (1999).
- [35] J. K. Morgan, *J. Geophys. Res.* **104**, 2721 (1999).
- [36] H. Hayakawa, *Progress of Theoretical Physics Suppl.* **138**, 537 (2000).
- [37] P. Jalali, W. Polashenski, T. Tynjälä, and P. Zamankhan, *Physica D* **162**, 188 (2002).
- [38] E. Aharonov and D. Sparks, *Phys. Rev. E* **65**, 051302 (2002).
- [39] C. S. Campbell, *J. Fluid Mech.* **465**, 261 (2002).
- [40] D. Volfson, L. S. Tsimring, and I. Aranson, *Phys. Rev. E* **68**, 021301 (2003).
- [41] I. Iordanoff and M. M. Khonsari, *J. Tribology* **126**, 137 (2004).
- [42] G. Lois, A. Lemaitre, and J. M. Carlson (2005), cond-mat/0501535.
- [43] K. L. Johnson, *Contact Mechanics* (Cambridge University Press, Cambridge, 1985).
- [44] N. Brilliantov, F. Spahn, J. M. Hertzsch, and T. Pöschel, *Phys. Rev. E* **53**, 5382 (1996).
- [45] S. Schollmann, *Phys. Rev. E* **59**, 889 (1999).
- [46] P. A. Cundall and O. D. L. Strack, *Géotech.* **29**, 47 (1979).
- [47] S. L. Silbert, D. Ertas, G. S. Grest, T. Halsey, D. Levine, and S. J. Plimpton, *Phys. Rev. E* **64**, 385 (2001).
- [48] J. N. Roux and F. Chevoir, *Bulletin des Laboratoires des Ponts et Chaussées* (2005), to be published.
- [49] M. P. Allen and D. J. Tildesley, *Computer simulation of liquids* (Oxford University Press, Oxford, 1987).
- [50] F. da Cruz, F. Chevoir, J. N. Roux, and I. Iordanoff, in *Transient Processes in Tribology*, edited by G. Dalmaz, A. A. Lubrecht, D. Dowson, and M. Priest (2004).
- [51] F. Calvetti, G. Combe, and J. Lanier, *Mech. Cohes. Frict. Mat.* **2**, 121 (1997).
- [52] E. Azanza, Ph.D. thesis, Ecole Nationale des Ponts et Chaussées, Paris (1998), in French.
- [53] D. Howell, R. Behringer, and C. Veje, *Chaos* **9**, 559 (1999).
- [54] M. Lätzel, S. Luding, and H. J. Hermann, *Granular Matter* **2**, 123 (2000).
- [55] M. Prochnow, Ph.D. thesis, Ecole Nationale des Ponts et Chaussées (2002), in French.
- [56] G. K. Batchelor, *J. Fluid Mech.* **41**, 545 (1970).
- [57] J. Christoffersen, M. M. Mehrabadi, and S. Nemat-Nasser, *J. Appl. Mech.* **48**, 339 (1981).
- [58] N. Kruyt and L. Rothenburg, *J. Appl. Mech.* **118**, 706 (1996).
- [59] J.-J. Moreau, in *Friction, Arching, Contact Dynamics*, edited by D. E. Wolf and P. Grassberger (World Scientific, Londres, 1997), pp. 233–247.
- [60] C. Goujon, N. Thomas, and B. Dalloz-Dubrujeaud, *Euro. Phys. J. E* **11**, 147 (2003).
- [61] G. Chambon, J. Schmittbuhl, A. Corfdir, J.-P. Vilotte, and S. Roux, *Phys. Rev. E* **68**, 011304 (2003).
- [62] G. Ovarlez and E. Clément, *Phys. Rev. E* **68**, 031302 (2003).
- [63] S. B. Savage and M. Sayed, *J. Fluid Mech.* **142**, 391 (1984).
- [64] M. Hanes and D. Inman, *J. Geophys. Res.* **90**, 3670 (1985).
- [65] K. Craig, R. H. Buckholz, and G. Domoto, *J. Appl. Mech.* **53**, 935 (1986).
- [66] C. S. Campbell, C. P. W., and H. M., *J. Geophys. Res.* **100**, 8267 (1995).
- [67] A. V. Potapov and C. S. Campbell, *Phys. Fluids* **8**, 2884 (1996).
- [68] J. Klausner, D. Chen, and R. Mei, *Powder Tech.* **112**, 94 (2000).
- [69] O. Pouliquen, *Phys. Fluids* **11**, 542 (1999).
- [70] O. Pouliquen and Y. Forterre, *J. Fluid Mech.* **453**, 133 (2002).
- [71] F. da Cruz, M. Prochnow, J.-N. Roux, and F. Chevoir, in *Powders and Grains* (2005).

- [72] R. A. Bagnold, Proc. Roy. Acad. London A **225**, 49 (1954).
- [73] L. Bocquet, W. Losert, D. Schalk, T. C. Lubensky, and J. P. Gollub, Phys. Rev. E **65**, 011307 (2002).
- [74] L. Bocquet, J. Errami, and T. C. Lubensky, Phys. Rev. Lett. **89**, 184301 (2002).
- [75] P. C. Johnson and R. Jackson, J. Fluid Mech. **176**, 67 (1987).
- [76] L. S. Mohan, P. R. Nott, and K. K. Rao, Chem. Eng. Sci. **52**, 913 (1997).
- [77] S. B. Savage, J. Fluid Mech. **377**, 1 (1998).
- [78] C. Ancey, Phys. Rev. E **65**, 11304 (2001).
- [79] J. N. Roux (2004), condmat 0405358.
- [80] V. K. Horvath, I. M. Janosi, and V. P. J., Phys. Rev. E **54**, 2005 (1996).
- [81] D. M. Hanes, J. T. Jenkins, and M. W. Richman, J. Appl. Mech. **55**, 969 (1988).
- [82] F. Radjai and S. Roux, in *Powders and grains*, edited by Y. Kishino (Lisse, Swets and Zeitlinger, Sendai, Japan, 2001), pp. 21–24.
- [83] S. Nasuno, A. Kudrolli, A. Bak, and J. P. Gollub, Phys. Rev. E **58**, 2161 (1998).
- [84] M. Lubert and A. de Ryck, Phys. Rev. E **63**, 021502 (2001).
- [85] F. da Cruz, F. Chevoir, D. Bonn, and P. Coussot, Phys. Rev. E **66**, 051305 (2002).
- [86] D. Mueth, Phys. Rev. E **67**, 011304 (2003).
- [87] D. Bonamy, F. Daviaud, L. Laurent, M. Bonetti, and J.-P. Bouchaud, Phys. Rev. Lett. **89**, 034301 (2002).
- [88] A. Ferguson, B. Fisher, and B. Chakraborty, Europhys. Lett. **66**, 277 (2003).
- [89] O. Pouliquen, Phys. Rev. Lett. (2004), to be published.
- [90] P. Mills, D. Loggia, and M. Tixier, Europhys. Lett. **45**, 733 (1999).
- [91] O. Pouliquen and Y. Forterre, Advances in complex systems **4**, 441 (2001).
- [92] D. Ertas and T. C. Halsey, Europhys. Lett. **60**, 931 (2002).
- [93] J. Rajchenbach, Phys. Rev. Lett. **90**, 144302 (2003).
- [94] M. Z. Bazant, J. Choi, and C. H. Rycroft (2003), condmat 0307379.
- [95] P. Mills, P. G. Rognon, and F. Chevoir, in *Powders and Grains* (2005).
- [96] O. Pouliquen, M. Belzons, and M. Nicolas, Phys. Rev. Lett. **91**, 014301 (2003).
- [97] C. Denniston and H. Li, Phys. Rev. E **59**, 3289 (1999).
- [98] M. R. Kuhn and K. Bagi, J. Eng. Mech. **130**, 826 (2004).
- [99] F. Radjai, in *Powders and Grains*, edited by Y. Kishino (Lisse, Swets and Zeitlinger, Sendai, Japan, 2001), pp. 157–160.
- [100] C. O’Hern, S. A. Langer, A. J. Liu, and S. R. Nagel, Phys. Rev. Lett. **86**, 111 (2001).
- [101] D. Z. Zhang and A. Rauenzahn, J. Rheol. **44**, 1019 (2000).
- [102] J.-N. Roux, Phys. Rev. E **61**, 6802 (2000).
- [103] L. Staron, J.-P. Vilotte, and F. Radjai, Phys. Rev. Lett. **89**, 204302 (2002).
- [104] K. I. Kanatani, Powder Tech. **28**, 167 (1981).
- [105] B. Cambou, P. Dubujet, F. Emeriault, and F. Sidoroff, Eur. J. Mech. A **14**, 255 (1995).
- [106] P. G. Rognon, M. Naaim, J. N. Roux, and F. Chevoir, in *Powders and grains* (2005).
- [107] J. C. Tsai, G. A. Voth, and J. P. Gollub, Phys. Rev. Lett. **91**, 064301 (2004).